Shape Optimization for Two-Dimensional Transonic Airfoil by Using the Coupling of FEM and BEM

Von der Fakultät für Mathematik und Physik der Universität Stuttgart
zur Erlangung des Würde eines
Doktors der Naturwissenschaften (Dr. rer. nat.)
genehmigte Abhandlung

vorgelegt von

M.Sc. Chol Gyu O

aus Pjoenjang

Hauptberichter:	Prof. Dr.-Ing. Dr. h.c. Wolfgang L. Wendland
Mitberichter:	Prof. Dr. rer. nat. Claus-Dieter Munz

Tag der mündlichen Prüfung: 23. Mai 2006

Institut für Angewandte Analysis und Numerische Simulation
Universität Stuttgart

2006

Contents

Acknowledgement

The present work was prepared during my stay in the Institute for Applied Analysis and Numerical Simulation at the Department of Mathematics, University of Stuttgart by the support of the Gottlieb Daimler- und Karl Benz-Stiftung with grant No. 02-01/03.
I would like to express my sincere thanks to the Gottlieb Daimler- und Karl Benz-Stiftung.
I express my deep gratitude to Prof. Dr.-Ing. Dr. h.c. Wolfgang L. Wendland for his valuable advices, discussions and efforts during the preparation of this thesis.
This thesis is based on the research work of Prof. W. L. Wendland and his partners including Prof. G. Warnecke, Dr. H. Berger, Prof. Dr. U. Göhner and Dr. C. A. Coclici from 1986 to 2000. Especially, Prof. W. L. Wendland and Dr. Coclici offered me their research results and software concerning for the computation of transonic flow problems, this enabled me to complete this thesis in due time.
I am grateful to Dr. Heiko Schulz, who helped me truely concerning the computer, so that I could do all computational works without any difficulty.
I express my sincere gratitude to Prof. Dr. Claus-Dieter Munz and Dr.-Ing. Thorsten Lutz in the Institute of Aerodynamics and Gasdynamics, University of Stuttgart.
When I had a poblem associated with my research stay, they let me to continue to perform my research project and offered a series of research results for the shape optimization of transonic airfoils.
I would like to thank all the members including secretary Ms. Ingrid Bock in the chair of applied mathematics, department of mathematics, University of Stuttgart.
I also dedicate my special greeting to Dr. Werner Kolbe and his family.

1 Introduction

All the organism and bodies around us lie and move in fluids. The fluid as the continuum of time and space are continuously moving. Without fluids we can not think about our life. The air and water that we drink everyday are fluids, and the blood flow in the body of organism is also a fluid. Fluid is an important resource of energy, too. Fluid gives not only the benefits to us, but also damages. For example, there are various accidents due to hurricanes and snowslides in several regions of the world in recent years. Investigating the phenomena of fluids exactly and handling it well is the forever task of human being.

Especially, the study of transonic flows is the centre of attention for many specialists. It has a great importance in the design of high speed aircraft and highly efficient turbines, compressors and other blade machines with large output.
Here we concentrate on the transonic fluid flow around an airfoil.

$\triangle$ There exist several mathematical models for the investigation of irrotational inviscid transonic flows.
The transonic potential equation is nonlinear and of mixed type due to ellipticity in the subsonic regions and hyperbolicity in the supersonic regions so that the mathematical treatment of this problem is more complicated than subsonic irrotational inviscid flows, where the solvability of boundary value problems for the velocity potential can be proved by the use of monotone operator theory.
Feistauer and Nečas [16] constructed a functional, whose minimization is equivalent to the solution of the irrotational inviscid transonic flow problem, with the use of the secant-modulus method and a convinient optimal control principle. They proved that if a minimizing sequence of the functional satisfies the entropy and bounded velocity conditions and converges weakly to a function u, then it converges strongly to u and u is a solution of the transonic flow problem.
The transonic flow problem can be handled as a variational inequality in a convex set which is given by a suitable entropy conditon, by a bound for the gas velocity and boundary conditions for the velocity potential [21].
During two decades, there was a great progress in the numerical computations of the transonic flow problems [2], [3], [4], [5], [6], [13], [14], [23], [24], [25], [38].
Mandel and Nečas [38] and Berger [2] transformed the finite element approximation of the full potential problem to a discrete minimization problem and proved its convergence for the subsonic and transonic cases to the continuous problem under the assumption of the uniqueness and existence of the soultion of the continuous problem. On the basis of previous finite element convergence, Berger, Warnecke and Wendland [6] constructed the numerical algorithm for the transonic flow problem by a finite element method and obtained good numerical results using that algorithm.
For the accuarate computations it needs to catch the exact position of the shock wave and to reconstruct the mesh generation around the shock wave. Göhner and Warnecke [24], [25] derived a shock indicator and a second order finite difference

error indicator available to catch the position of the shock wave, and using these indicator proposed a computational algorithm by the adaptive h, r finite element approximation.
So far, when treating the far-field problem, most of flow problems were formulated in a sufficiently large computational domain and the velocity at infinity was chosen as the boundary condition of the domain, which requires expensive computational costs. It was necessary to describe the far-field condition exactly and to reduce the computational costs.
Base on the numerical results in the bounded domain by the finite element method, there were various approaches for the transonic flow problem in an unbounded domain by using the coupled FEM and BEM and some domain decomposition method [5], [12], [13], [14]. Berger, Warnecke and Wendland [5] approximated the far field problem by the linearized Prandtl-Glauert equation, defined the variational problem using the coupled FEM and BEM, and arranged the computational basis for the transonic flow problem in an unbounded domain which allows to compute accurately with a cheap computational cost. Coclici [12] and Wendland [13] proved that if the Kutta-Joukowski condition is valid, the stress intensity factor at the trailing edge of the airfoil vanishes, and developed the faster and robust computational algorithm than previous one based on this analysis. These achievements in the computation of transonic flow problem are based on the recent development of the coupling of finite element and boundary element methods for the elliptic boundary value problem in an unbounded domain [9], [18], [19], [26], [35], [40].

$\triangle$ It enables us to implement the shape optimization for the transonic airfoil whose state equation is the full potential equation.
Since there was a mathematical definition of the shape optimization three decades ago [10], [32], the mathematical approaches for the shape optimization now play a crucial role in the aerodynamical design. The design of good aerodynamical shapes is an important problem for the designers of turbomachines and aircrafts. Many scientists of different disciplines have contributed to this field [1], [7], [8], [20], [36], [37], [42], [45], [49], [50], [53]. Finite elements and nonlinear optimization for the shape optimization of compressible subsonic flows have been used by Angrand [1] who computed optimal shapes of a nozzle and a lifting airfoil by using the full potential equation. The feasibility of the finite element and nonlinear optimization methods in solving optimal design problems for transonic potential flow under the assumption of a smooth shock wave was studied by Mäkinen [36], [37].
One of the crucial issues in the aerodynamical shape optimization is to devise a method for the body surface representation which can generate physically realistic shapes with as few design variables as possible. Sohn and Lee [45] developed a semi-analytical algorithm to determine the control points of a Bezier curve which can reproduce the initial shape accurately with a minimum number of control points, they proposed new sets of design variables to overcome the dependency of the side constraints on the initial geometry and applied it to the Navier-Stokes equation.

A number of numerical experiments in which different Bezier parameterizations of an airfoil have been construced and compared, in the context of curvefitting first, and then as part of an adaption step within an aerodynamic optimization were conducted by Tang and Désidéri [53].
In relation with the computation for Navier-Stokes aerodynamic shape optimization, Burgreen and O. Baysal [8], Nemec and Zingg [42] obtained the gradient of the objective function via the discrete adjoint and flow-sensitivity methods. The adjoint and flow-sensitivity equations were solved using a preconditioned GMRES solver. The performance of a new algorithm was demonstrated for several design problems, such as inverse design, lift-constrained drag minimization, lift enhancement and maximization of lift-to-drag ratio.
Aerodynamic efficiency at off-design conditions can be improved by the application of a shock control bump on a variable camber airfoil.
Sommerer, Lutz and Wagner [49], [50] proposed a computational algorithm for the design of a shock control bump to be properly shaped and positioned in order to generate a favourable effect by using a hybrid optimiser, a geometry module and a coupled Euler-boundary layer code. Shape optimization for an adaptive bump were carried out for different Mach numbers at a fixed lift coefficient.
In order to derive the shape sensitivity of the transonic full potential equation, it is necessary to study the sensitivity of the boundary value problem including the inequality constraint because of the entropy condition. There exist a lot of contributions to the shape sensitivity of the variational inequality based on the penalty approximation [27], [28], [29], [30], [31], [41], [46], [47], [48].

$\triangle$ Throughout this paper will be considered the following topics:
• Development of a computational algorithm of the full potential equation for the shape optimization.
• Choice of entropy and penalty parameters depending on the shape of the transonic airfoil.
• Approximation of the discrete minimization problem for the coupled FEM and BEM by a second order differentiable problem and its convergence.
• Bezier parameterization of the design variables with only few Bezier control points.
• Sensitivity analysis for the coupling boundary value problem.
• Development of a computational algorithm for the shape optimization of a transonic airfoil in $\mathbb{R}^2$.
• Derivation of numerical experiments.

This paper consists of two sections:
In section 1 we consider the mathematical model of the transonic flow problem, its variational formulation and solution. The mathematical model is derived from the system of conservation laws and this model is converted to the coupling boundary value problem in which the full potential equation near the body is coupled with the linear Prandtl-Glauert model in the far field. The discrete variational problem for the coupled problem is described by a discrete minimization problem and the

computational algorithm is formulated. In the last part of this section we present a second order differentiable approximation for the minimizing functional and show its convergence to the continuous coupled problem.
In section 2 we deal with the shape optimization for the transoinc airfoil by using the coupling FEM and BEM.
First of all, we derive the airfoil parameterization by some Bezier curve. An algorithm for the airfoil reconstruction by Bezier curve and some numerical results are derived. Then we present the shape sensitivity analysis formula by using the discrete adjoint state technique. Based on this analysis, the computational algorithm for the transonic airfoil by using the coupling of FEM and BEM is employed and some numerical relsults are shown.

2 The computation of 2D transonic flow by the coupling of FEM and BEM

In this chapter we consider the derivation of the full potential equation from the system of conservation laws, its variational formulation and the application the coupling method of FEM and BEM to this problem. Moreover, we give some computational results based on the computational algorithm by the discrete minimization.

2.1 The derivation of the full potential equation

The motion of fluid flows is governed by the fundamental physical laws of conservation of mass, momentum and energy, the so-called system of conservation laws. Since the number of unknown flow variables is lager than the number of equations, the system is appended by constitutive relations and thermodynamical state equations.
Let us denote by $\Omega \in \mathbb{R}^n (n = 2, 3)$ the region occupied by the fluid and let $[t_0, T)$ be a time interval, $0 < t_0 < T$.
Let us introduce some symbols.

$\mathbb{X} = (x_1, \cdots, x_n)^T$: an arbitray point in Ω

$\varrho = \varrho(\mathbb{X}, t),\ P = P(\mathbb{X}, t)$: density and pressure, respectively

$\mathbb{V} = \mathbb{V}(\mathbb{X}, t) = (v_1(\mathbb{X}, t), \cdots, v_n(\mathbb{X}, t))^T$: velocity vector

$\theta = \theta(\mathbb{X}, t)$: absolute temperature

$\mathbb{F} = \mathbb{F}(\mathbb{X}, t) = (f_1(\mathbb{X}, t), \cdots, f_n(\mathbb{X}, t))^T$: external force

$q = q(\mathbb{X}, t)$: the density of external heat resource

$\mathbb{Q} = \mathbb{Q}(\mathbb{X}, t)$: heat flux

$\lambda,\ \mu$: coefficients of viscosity

k : heat conductive coefficient

c_P : specific heat at constant pressure

c_V : specific heat at constant volume

$E = E(\mathbb{X}, t)$: the density of the total specific energy

$U,\ S$: the density of the internal energy and the entropy, respectively

The system of conservation laws is written as the following system of equations:

$$\begin{aligned}
&\frac{\partial \varrho}{\partial t}+\sum_{j=1}^{n}\frac{\partial(\varrho v_j)}{\partial x_j}=0\\
&\frac{\partial(\varrho v_i)}{\partial t}+\sum_{j=1}^{n}\varrho v_j\frac{\partial v_i}{\partial x_j}=\varrho f_i-\frac{\partial P}{\partial x_i}+\lambda\frac{\partial(div\mathbb{V})}{\partial x_i}+\mu\sum_{j=1}^{n}\frac{\partial}{\partial x_j}[\frac{\partial v_i}{\partial x_j}+\frac{\partial v_j}{\partial x_i}], i=1,\cdots,n\\
&c_V(\varrho\frac{\partial\theta}{\partial t}+\varrho\ grad\ \theta\cdot\mathbb{V})=div(k\ grad\ \theta)-Pdiv\mathbb{V}+\lambda(div\mathbb{V})^2\\
&\qquad+\frac{\mu}{2}\sum_{i,j=1}^{n}[\frac{\partial v_i}{\partial x_j}+\frac{\partial v_j}{\partial x_i}]^2+\varrho\mathbb{F}\cdot\mathbb{V}+\varrho q.
\end{aligned}\tag{2.1}$$

In these equations $\varrho, \mathbb{V}$ and θ are unknowns. The pressure P becomes a known variable because it is represented by the state equation $P=(c_P-c_V)\varrho\theta$. The system of equations describes the motion of unsteady, compressible, viscous fluid flows, and it is called the Navier-Stokes equations. Now we derive the equation that will be considered in this paper. We suppose the fluid flow inviscid and adiabatic, i.e., the heat transmission and heat exchange between fluid volumes are zero. Note that in adiabatic flow the heat sources and heat fluxes are zero, therefore $q=0$, $\mathbb{Q}=0$. Under these assumptions, we obtain the hyperbolic system of Euler equations describing the motion of unsteady, compressible, inviscid fluid flows:

$$\begin{aligned}
&\frac{\partial \varrho}{\partial t}+\sum_{j=1}^{n}\frac{\partial(\varrho v_j)}{\partial x_j}=0\\
&\frac{\partial(\varrho v_i)}{\partial t}+\sum_{j=1}^{n}\varrho v_j\frac{\partial v_i}{\partial x_j}=\varrho f_i-\frac{\partial P}{\partial x_i}, i=1,\cdots,n\\
&c_V(\varrho\frac{\partial\theta}{\partial t}+\varrho\ grad\ \theta\cdot\mathbb{V})=\varrho\mathbb{F}\cdot\mathbb{V}-Pdiv\mathbb{V}.
\end{aligned}\tag{2.2}$$

If it is assumed that the motion of fluid flow in the 2D region is steady and that external forces vanish, then the system of equations (2.2) become the steady Euler equations:

$$div(\varrho\mathbb{V})=0\quad\text{in }\Omega \tag{2.3}$$

$$\sum_{j=1}^{2}v_j\frac{\partial\mathbb{V}}{\partial x_j}=-\frac{1}{\varrho}grad\ P \tag{2.4}$$

$$div[\varrho\mathbb{V}(E+\frac{P}{\varrho})]=0. \tag{2.5}$$

Using (2.4) and the entropy relation $\theta ds=dU-\frac{P}{\varrho^2}d\varrho$, we obtain

$$-\mathbb{V}\times rot\mathbb{V}=-grad\ [E+\frac{P}{\varrho}]+\theta\nabla S. \tag{2.6}$$

From (2.3) and (2.5) we find

$$\mathbb{V}\cdot grad\ (E+\frac{P}{\varrho})=0. \tag{2.7}$$

Additionally, the flow is supposed to be isoenergetic, $\nabla S = 0$ and

$$grad\ [E + \frac{P}{\varrho}] = 0 \quad \text{in } \Omega. \tag{2.8}$$

Therefore, in the case of 2-dimensional space under the above assumptions the fluid flow is irrotational:

$$rot\mathbb{V} = 0. \tag{2.9}$$

Moreover, in the case of 2-dimensional irrotational flow

$$\frac{1}{\varrho} grad\ P + grad\ [\frac{|\mathbb{V}|^2}{2}] = 0. \tag{2.10}$$

In the case of homentropic flow, the following relation holds between the pressure and the density:

$$P = P_0(\frac{\varrho}{\varrho_0})^\kappa, \tag{2.11}$$

where $\kappa := \dfrac{c_P}{c_V}$ is the Poisson adiabatic constant, P_0 and ϱ_0 are the pressure and the density for the motionless gas. From (2.10) and (2.11)

$$grad\ [\frac{\kappa}{\kappa - 1}\frac{P_0}{\varrho_0^\kappa}\varrho^{\kappa-1} + \frac{|\mathbb{V}|^2}{2}] = 0 \quad \text{in } \Omega. \tag{2.12}$$

Integrating the above equality in Ω it is obtained Bernoulli equation

$$\frac{\kappa}{\kappa - 1}\frac{P_0}{\varrho_0^\kappa}\varrho^{\kappa-1} + \frac{|\mathbb{V}|^2}{2} = \frac{\kappa}{\kappa - 1}\frac{P_0}{\varrho_0^\kappa}\varrho_0^{\kappa-1}. \tag{2.13}$$

Using the fact that the local speed of sound in motionless gas is given by

$$a_0^2 = \frac{\kappa P_0}{\varrho_0}, \tag{2.14}$$

from (2.13) we obtain the following relation between density and velocity:

$$\varrho = \varrho(|\mathbb{V}|^2) = \varrho_0(1 - \frac{\kappa - 1}{2a_0^2}|\mathbb{V}|^2)^{\frac{1}{\kappa-1}}. \tag{2.15}$$

Thus the continuity equation (2.3) can be rewritten in terms of some velocity potential u in the form

$$div[\varrho(|grad\ u|^2)grad\ u] = 0 \quad \text{in } \Omega. \tag{2.16}$$

This equation is the full potential equation describing a stationary, compressible, homentropic, isoenergetic, two-dimensional flow of an inviscid fluid. Further we will consider the shpae optimization whose state equation is the full potential equation.

2.2 The mathematical model

Let $\Omega \subset \mathbb{R}^2$ be an open bounded domain surrounding a given simply connected wing surface $P \subset \mathbb{R}^2$. The boundary of Ω consists of three parts

$$\partial\Omega := \Gamma_\infty \cup \Gamma_p \cup \Sigma,$$

whose interiors are mutually disjoint and where Γ_∞ and Γ_p are closed Jordan curves connected by Σ. The curve $\Gamma_\infty \in C^\infty$ is the artificial exterior boundary of Ω which is taken in order to obtain a bounded computational domain. The curve Γ_p is the common boundary between Ω and the profile P, which has a corner, the trailing edge (TE), and is C^∞ otherwise. We denote by Σ a slit in $\bar{\Omega}$, joining the trailing edge with Γ_∞. The unbounded far field domain exterior to Γ_∞ will be denoted by $\Omega^c = \mathbb{R}^2 \backslash \overline{\Omega \cup P}$.

The straight prolongation of the slit Σ in Ω^c to infinity will be denoted by Σ^c.

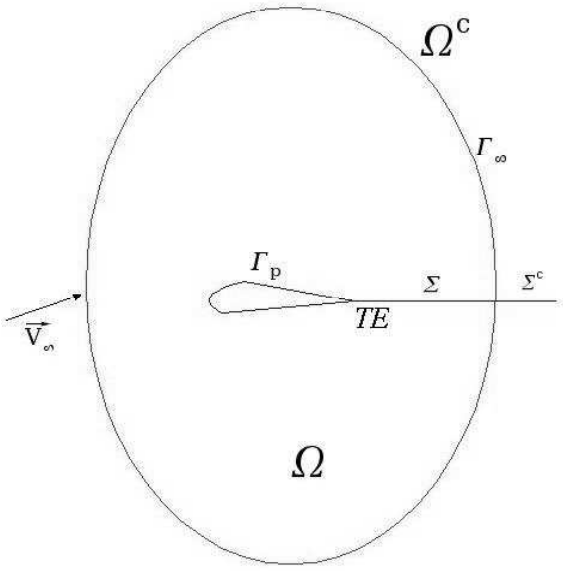

Figure 1: The geometry of the coupling problem.

The potential flow with the velocity $\vec{v} = \nabla u$ is governed by the full potential equation :

$$div[\varrho(|\nabla u|^2)\nabla u] = 0 \quad \text{in } \Omega. \tag{2.17}$$

The density function is represented as the following relation derived before,

$$\varrho(|\nabla u|^2) = \varrho_0(1 - \frac{\kappa - 1}{2a_0^2}|\nabla u|^2)^{\frac{1}{\kappa-1}}. \tag{2.18}$$

Here $\kappa > 1$ is the adiabatic gas constant, e.g. $\kappa = 1.4$ for dry air. The constants ϱ_0, a_0 are the density and the local speed of sound, respectively. The local speed of sound $a(|\nabla u|^2)$ is given by

$$[a(|\nabla u|^2)]^2 = a_0^2\varrho_0^{1-\kappa}[\varrho(|\nabla u|^2)]^{\kappa-1} = a_0^2 - \frac{\kappa - 1}{2}|\nabla u|^2 \tag{2.19}$$

and the local Mach number is $M := \frac{|\nabla u|}{a}$. Note that the density $\varrho(s)$ is only defined for $|\nabla u|^2 \leq \frac{2a_0^2}{\kappa-1}$. This bound for the velocity will be assumed to hold in all further considerations.

The equation (2.17) changes its type at the sonic flow speed $|\nabla u| = a = a^* := (\frac{2a_0^2}{\kappa+1})^{\frac{1}{2}}$, i.e. $M = 1$. For $|\nabla u| < a^*$, i.e. $M < 1$, it is elliptic and the velocity is subsonic. For $|\nabla u| > a^*$, i.e. $M > 1$, it is hyperbolic and the velocity is supersonic.

- The boundary condition on Σ

In order to have a potential flow with circulation and lift we introduce the slit Σ across which we assume that the velocity field ∇u is continuous, whereas the potential u has a finite constant jump. This implies

$$u^+ - u^- = \beta \quad \text{and} \quad \partial_n u^+ - \partial_n u^- = 0 \quad \text{on } \Sigma. \tag{2.20}$$

Here, $\vec{n}$ is a unit vector field on Σ and $\partial_n u = \nabla u \cdot \vec{n}$. By u^+, u^- we denote the one-sided boundary values on Σ. The constant β is an additional unknown and gives the circulation of the flow. To determine the jump β, we need the additional Kutta-Joukowski condition

$$F(\beta) = |\nabla u^+|^2_{TE} - |\nabla u^-|^2_{TE} = 0 \tag{2.21}$$

at the trailing edge TE which follows from the requirement of continuous pressure there. Here we shall assume that the flow near TE is subsonic which implies (2.21) too (see [13]).

- The boundary condition on the profile Γ_p

On the profile we impose the homogeneous Neumann boundary condition of non-penetration, which is equivalent to a vanishing mass flux, i. e.

$$\partial_n u = 0 \quad \text{on } \Gamma_p. \tag{2.22}$$

-The boundary condition on Γ_∞

For completeness, we still need a boundary condition at Γ_∞. It is generally assumed that a physically correct boundary condition for exterior flow is the requirement that the velocity $\vec{v}$ tends to the constant travelling velocity $\vec{v}_\infty$ at infinity. A simple and widely used method for approximating this condition is the following mass flux condition at Γ_∞, i.e.

$$\varrho(|\nabla u|^2)\partial_n u = \varrho(|\vec{v}|^2)\vec{v}_\infty \cdot \vec{n} \quad \text{on } \Gamma_\infty. \tag{2.23}$$

A slight improvement of (2.23) can be obtained by replacing $\vec{v}_\infty$ on the right-hand side by $\vec{v}_{0|\Gamma_\infty}$, where $\vec{v}_0$ is the velocity of the incompressible potential flow in $\Omega \cup \Omega^c \cup \Gamma_\infty$.

For the far field in Ω^c we take the linearized Prandtl-Glauert model. To this end let us denote by α_0 the angle of attack. Then, in the new coordinates $\tilde{x}_1, \tilde{x}_2$ with their complex notation

$$\tilde{x_1} + i\tilde{x_2} := ((x_1 - 1/2) + ix_2) \cdot e^{-i\alpha_0}$$

we have $\vec{v}_\infty = v_\infty \vec{e}_{1,x}$, whereas in the original coordinates in $\mathbb{C}$, $\vec{v}_\infty = v_\infty e^{i\alpha_0}$. Hence in the new coordinates, the Prandtl-Glauert approximation corresponds to

$$\partial u / \partial \tilde{x}_2 = 0$$

and therefore we use for the far field in Ω^c the linearized model equation

$$(1 - M_\infty^2)u_{\tilde{x}_1\tilde{x}_1} + u_{\tilde{x}_2\tilde{x}_2} = 0. \tag{2.24}$$

The perturbation potential φ is defined by

$$\varphi := u - \Psi \quad \text{with } \Psi(\tilde{x}, \beta) := \vec{v}_\infty \cdot (\tilde{x}_1, \tilde{x}_2) + \frac{\beta}{2\pi} \arctan \frac{\sqrt{1 - M_\infty^2} \cdot \tilde{x}_2}{\tilde{x}_1}, \tag{2.25}$$

where M_∞ is the Mach number at infinity. The function φ is continuously differentiable in Ω^c and satisfies

$$(1 - M_\infty^2)\varphi_{\tilde{x}_1\tilde{x}_1} + \varphi_{\tilde{x}_2\tilde{x}_2} = 0 \tag{2.26}$$

together with the radiation condition $\nabla\varphi(\tilde{x}) \to \vec{0}$ for $|\tilde{x}| \to \infty$ and the transmission conditions

$$\varphi^+ - \varphi^- = 0 \quad \text{and } \varrho(|\nabla\varphi^+|^2)\partial_{\tilde{n}}\varphi^+ - \varrho(|\nabla\varphi^-|^2)\partial_{\tilde{n}}\varphi^- = 0 \quad \text{on } \Sigma^c. \tag{2.27}$$

The coupling of the transonic flow in Ω and the exterior Prandtl-Glauert approximation is modelled by the continuity of the potential across Γ_∞ and by the mass flux condition

$$\varrho(|\nabla u|^2)\nabla u \cdot \vec{n} = \varrho_\infty\{\nabla\Psi \cdot \vec{\tilde{n}} + (1 - M_\infty^2)\varphi_{\tilde{x}_1}\tilde{n}_1 + \varphi_{\tilde{x}_2}\tilde{n}_2\} \quad \text{on } \Gamma_\infty, \tag{2.28}$$

where $\vec{n} = (n_1, n_2)$ and $\vec{\tilde{n}} = (\tilde{n}_1, \tilde{n}_2)$ represent the exterior unit normal vectors to Γ_∞ with respect to the initial and to the new coordinates, respectively. Collecting the equations (2.17),(2.20),(2.21),(2.22),(2.26),(2.27) and the coupling conditions (2.25),(2.28), we get the following system of equations, boundary and transmission conditions:

Coupled boundary value problem

find that u, φ in appropriate function spaces and the constant $\beta \in \mathbb{R}$ satisfying the

Interior full potential poblem

$$\begin{aligned} div[\varrho(|\nabla u|^2)\nabla u] = 0 \qquad & \text{in } \Omega, \\ \partial_n u = 0 \qquad & \text{on } \Gamma_p, \\ u^+ - u^- = \beta \qquad & \text{on } \Sigma, \\ \partial_n u^+ - \partial_n u^- = 0 \qquad & \text{on } \Sigma, \\ F(\beta) = |\nabla u^+|^2_{TE} - |\nabla u^-|^2_{TE} = 0; & \end{aligned} \tag{2.29}$$

Exterior Prandtl-Glauert problem,

$$\begin{aligned} (1 - M_\infty^2)\varphi_{\tilde{x}_1\tilde{x}_1} + \varphi_{\tilde{x}_2\tilde{x}_2} = 0 \qquad & \text{in } \Omega^c, \\ \nabla\varphi = 0(1) \qquad & \text{for } |\tilde{x}| \to \infty, \\ \varphi^+ - \varphi^- = 0 \qquad & \text{on } \Sigma^c, \\ \partial_n\varphi^+ - \partial_n\varphi^- = 0 \qquad & \text{on } \Sigma^c; \end{aligned} \tag{2.30}$$

Coupling conditions,

$$u = \varphi + \Psi \quad \text{on } \Gamma_\infty \tag{2.31}$$

and

$$\varrho(|\nabla u|^2)\partial_n u = \varrho(|\vec{v}_\infty|^2)\{\nabla\Psi \cdot \vec{\tilde{n}} + ((1 - M_\infty^2)\varphi_{\tilde{x}_1}, \varphi_{\tilde{x}_2}) \cdot \vec{\tilde{n}}\} \quad \text{on } \Gamma_\infty. \tag{2.32}$$

Note that, for a solution (u, φ, β) of this coupled problem(2.31)-(2.34), one also has the solution $(u + c, \varphi + c, \beta)$ with an arbitrary constant c. We therefore fix this constant by the requirement

$$\int_{\Gamma_\infty} \varphi ds = 0.$$

The entropy condition

For the case in which the geometry of the problem and the boundary conditions lead to a locally supersonic flow near the profile, the situation changes quite dramatically. In the supersonic regions the equation (2.17) becomes hypebolic and the monotonicity property is lost. In this case the existence of solutions to the above

problem is still open, even for problems with bounded domains. A further complication comes from the fact that the solutions have discontinuous derivatives ∇u, i.e. contain shocks. Hence, one has to consider weak solutions which in turn lead to nouniqueness and the existence of non-physical solutions. Therefore we will focus on the specific entropy condition [24]. Due to the assumption of isentropy, the shocks in transonic potential flow conserve entropy but not momentum.

The appropriate entropy condition (see [34]) requires that the divergence of the flow field must be bounded from above, i.e.

$$div(grad\ u) \leqslant B \quad \text{with an appropriate constant } B \in \mathbb{R}. \tag{2.33}$$

In Göhner and Warnecke [24] it is shown that this inequality is equivalent to the solution with compressive shocks and is violated by the non-physical expansion shocks. In weak form this means that the inequality

$$\int_\Omega \nabla u \cdot \nabla \psi dx \leqslant B \int_\Omega \psi dx \quad \text{for all } \psi_0^\infty(\Omega) \quad \text{with } \psi \geqslant 0 \tag{2.34}$$

must hold.

2.3 The variational formulation

Let $W^{s,p}(\Omega), s \in \mathbb{R}$, $p \in [1, \infty]$ and $W^{s,p}(\Gamma_\infty)$ be the usual Sobolev spaces equipped with norms $\|\cdot\|_{W^{s,p}(\Omega)}$ and $\|\cdot\|_{W^{s,p}(\Gamma_\infty)}$, respectively. We define $\langle\cdot,\cdot\rangle$ to be the duality pairing between $H^s(\Gamma_\infty) := W^{s,2}(\Gamma_\infty)$ and the dual space $H^{-s}(\Gamma_\infty)$ with respect to the $L^2(\Gamma_\infty)$ inner product,

$$\langle \chi, \psi \rangle := \int_{\Gamma_\infty} \chi(s)\psi(s)ds \quad \text{for all } (\chi, \psi) \in H^s(\Gamma_\infty) \times H^{-s}(\Gamma_\infty).$$

We further introduce the spaces

$$\begin{aligned} V &:= \{v \in W^{1,2}(\Omega) | v^+ - v^- = \beta \text{ on } \Sigma, \quad \beta \in \mathbb{R}\}, \\ V^0 &:= \{v \in W^{1,2}(\Omega) | v^+ - v^- = 0 \text{ on } \Sigma\}, \\ H &:= \left\{ \psi \in H^{-\frac{1}{2}}(\Gamma_\infty) | \int_{\Gamma_\infty} \psi ds = 0 \right\}, \end{aligned} \tag{2.35}$$

and the set of admissible functions

$$K_{s_0} := \left\{ v \in V | \quad |\nabla v|^2 \leqslant s_0 < \frac{2a_0^2}{\kappa - 1} \quad \text{a.e. in } \Omega \right\}, \tag{2.36}$$

K_{s_0} is a closed, convex subset of V in $W^{1,2}(\Omega)$. In order to simplify the notations we define the following nonlinear form

$$a(u|v, w) := \int_\Omega \varrho(|\nabla u|^2)\nabla v \cdot \nabla w dx \quad \text{for all triplets } (u, v, w) \in K_{s_0} \times V \times V.$$

For soving the exterior problem (2.32), we shall use a boundary potential formulation based on the Green representation theorem. To this end, one transforms the Prandtl-Glauert equation in (2.32) with constant coefficients into Laplace's equation and then uses classical potential theory. One obtains with the fundamental solution

$$G(\tilde{x}, \tilde{y}) := \frac{1}{2} log|(\frac{1}{\sqrt{1 - M_\infty^2}}[\tilde{x}_1 - \tilde{y}_1], [\tilde{x}_2, \tilde{y}_2])| \tag{2.37}$$

and the kernel of the double layer potential

$$K(\tilde{x}, \tilde{y}) := \frac{1}{2\pi} \frac{([\tilde{x}_1 - \tilde{y}_1], [\tilde{x}_2 - \tilde{y}_2]) \cdot \vec{\tilde{n}}(y)}{|(\frac{1}{\sqrt{1-M_\infty^2}}[\tilde{x}_1 - \tilde{y}_1], [\tilde{x}_2 - \tilde{y}_2])|^2} \tag{2.38}$$

the Green representation formula in the form

$$\begin{aligned} \varphi(\tilde{x}) = &\frac{\epsilon}{\sqrt{1 - M_\infty^2}} \int_{\Gamma_\infty} \{(1 - M_\infty^2)\varphi_{\tilde{y}_1}\tilde{n}_1(\tilde{y}) + \varphi_{\tilde{y}_2}\tilde{n}_2(\tilde{y})\} G(\tilde{x}, \tilde{y}) ds_{\tilde{y}} \\ &+ \frac{\epsilon}{\sqrt{1 - M_\infty^2}} \int_{\Gamma_\infty} \varphi(\tilde{y}) K(\tilde{x}, \tilde{y}) ds_{\tilde{y}} + \varphi_\infty \end{aligned} \tag{2.39}$$

with $\epsilon = 1$ for $\tilde{x} = (\tilde{x}_1, \tilde{x}_2) \in \Omega^c$ and $\epsilon = 2$ for $\tilde{x} \in \Gamma_\infty$.

We introduce the co-normal derivative of φ on Γ_∞ by

$$\lambda(\tilde{x}) = \varrho(|\vec{v}_\infty|^2)\{(1 - M_\infty^2)\varphi_{\tilde{x}_1}\tilde{n}_1(\tilde{x}) + \varphi_{\tilde{x}_2}\tilde{n}_2(\tilde{x})\}. \tag{2.40}$$

Further, we will denote the new coordinates $\tilde{x} = (\tilde{x}_1, \tilde{x}_2)$ by $x = (x_1, x_2)$.

Then the Green representation formula can be rewitten in the form

$$\begin{aligned} \varphi(x) = &\frac{\epsilon}{\sqrt{1 - M_\infty^2}\varrho(|\vec{v}_\infty|^2)} \int_{\Gamma_\infty} G(x, y)\lambda(y)ds_y \\ &+ \frac{\epsilon}{\sqrt{1 - M_\infty^2}} \int_{\Gamma_\infty} K(x, y)\varphi(y)ds_y + \varphi_\infty. \end{aligned} \tag{2.41}$$

We define the boundary integral operators of single and double layer potentials

$$\begin{aligned} \mathcal{V}\lambda(x) &:= -\int_{\Gamma_\infty} \frac{2G(x, y)}{\varrho(|\vec{v}_\infty|^2)\sqrt{1 - M_\infty^2}}\lambda(y)ds_y, \\ \mathcal{K}\varphi(x) &:= \int_{\Gamma_\infty} \frac{2K(x, y)}{\sqrt{1 - M_\infty^2}}\varphi(y)ds_y. \end{aligned} \tag{2.42}$$

Thus, for $x \in \Gamma_\infty$ we may write (2.41) in short as

$$\varphi(x) + \mathcal{V}\lambda(x) - \mathcal{K}\varphi(x) = 2\varphi_\infty. \tag{2.43}$$

Further, we define the bilinear forms

$$b(\lambda, \psi) := \langle \mathcal{V}\lambda, \psi \rangle \quad \text{and } d(\lambda, \psi) := \langle \mathcal{K}\lambda, \psi \rangle$$

for $\lambda, \psi \in H^{-\frac{1}{2}}(\Gamma_\infty)$, and the functionals

$$l_1(v, \beta) := \varrho_\infty \langle \nabla\Psi(\cdot, \beta) \cdot \vec{n}, v \rangle$$

and

$$l_2(\psi, \beta) := \langle (\mathcal{I} - \mathcal{K}\Psi(\cdot, \beta), \psi \rangle$$

for all $v \in W^{\sigma,p}(\Omega)$ and all $\psi \in H^{-\frac{1}{2}}(\Gamma_\infty)$. For every fixed $\beta \in \mathbb{R}$, these are linear and bounded functionals.

If we multiply equation (2.43) by a test function $\psi \in H$ and integrate over Γ_∞,

we obtain

$$\langle \mathcal{V}\lambda, \psi \rangle + \langle \varphi, \psi \rangle - \langle \mathcal{K}\varphi, \psi \rangle = b(\lambda, \psi) + \langle \varphi, \psi \rangle - d(\varphi, \psi) = 0 \quad \text{for all } \psi \in H. \tag{2.44}$$

This is the weak formulation for the boundary integral equation (2.43).

The weak formulation for a solution of problem (2.29) can be obtained by the usual variational approach.

Find $u \in K_{s_0}$ and $\beta \in \mathbb{R}$ such that

$$a(u|u,v) - \langle \varrho|\nabla u|^2)\partial_n u, v\rangle = 0 \quad \text{for all } v \in V^0. \tag{2.45}$$

The coupling of the weak formulation (2.45) in Ω and (2.44) in Ω^c can be obtain with (2.33),(2.34) in variational form via the flux balance through Γ_∞.

Thus, we obtain the following variational formulation for the coupling problem.

Find the three quantities $(u, \lambda, \beta) \in K_{s_0} \times H \times \mathbb{R}$ such that

$$\begin{aligned} &a(u|u,v) - \langle \lambda, v\rangle = l_1(v,\beta) && \text{for all } v \in V^0 \\ &b(\lambda,\psi) + \langle u,\psi\rangle - d(u,\psi) = l_2(\psi,\beta) && \text{for all } \psi \in H^{-\frac{1}{2}}(\Gamma_\infty) \\ &F(\beta) = |\nabla u^+|^2_{TE} - |\nabla u^-|^2_{TE} = 0. \end{aligned} \tag{2.46}$$

For the Kutta Joukowski condition the following fact holds [13].

Theorem 2.1 *Let the trailing edge angle ω satisfy $0 < \omega < \pi$.*

Let $(u, \lambda, \beta) \in K_{s_0} \times H \times \mathbb{R}$ be the variational solution satisfying

$$a(u|u,v) - \langle \lambda, v\rangle = l_1(v,\beta) \quad \textit{for all } v \in V^0$$

$$b(\lambda,\psi) + \langle u,\psi\rangle - d(u,\psi) = l_2(\psi,\beta) \quad \textit{for all } \psi \in H.$$

Let us further assume that there exist some bound $s_{TE} \in (0, \frac{2a_0^2}{\kappa+1})$ and a radius $r_0 > 0$ such that around the trailing edge

$$|\nabla u(x)|^2 \leqslant S_{TE} \quad \textit{for all } x \in \mathcal{U} := \{x \in \bar{\Omega} || x - TE| < r_0\}, \tag{2.47}$$

i.e. the flow is subsonic around TE.

Then the velocity field ∇u is Hölder continuous in $\mathcal{U}$ and already satisfies the Kutta-Joukowski condition

$$\nabla u|^+_{TE} = \nabla u|^-_{TE}. \tag{2.48}$$

2.4 The coupled FEM-BEM formulation

In order to discretize the coupled problem (2.46), we approximate the domain Ω by a family of polygonal domains Ω_h where h denotes the parameter of meshwidth. The outer boundary Γ_∞^h of Ω_h is supposed to be a polygonal curve with nodes on Γ_∞ which approximates Γ_∞. In the same way we define Γ_P^h as the approximation of the profile boundary Γ_p. Without loss of generality we may assume that the slit Σ is aleady a part of the boundary of Ω_h (see Figure 2). Together with Ω_h we introduce now a family of regular triangulations $\{\mathcal{T}_h\}_{h>0}$ with $\mathcal{T}_h := \bigcup_{i\in D} T_i$ where D is a finite subset of the natural numbers $\mathbb{N}$. The nodal points of the triangulation are denoted by $p_i, i = 1, \cdots, N$. For convenience we assume that the nodes on the slit Σ will be taken to be the first $2L$ points, i.e. $p_j^+, p_j^-, j = 1, \cdots, L$, with p_j^+ and p_j^- having the same coordinates but characterizing the limits from above and below, respectively.

By $\omega_{h_i}, i = 1, \cdots N$, we denote the usual piecewise linear hat functions satisfying $\omega_{h_i}(p_j) = \delta_{ij}$, $i, j = 1, \cdots, N$, which form a basis of nonnegative functions for the piecewise linear continuous finite elements. By A_i we denote the areas of the corresponding supports, i.e. $A_i = meas(\text{supp } \omega_{h_i}), i = 1, \cdots, N$.

For a triangle $T_i \in \mathcal{T}_h$ let α_i denote the smallest angle. We say that a family of regular triangulations $\{\mathcal{T}_h\}_{h>0}$ satisfies the angle property if there is a minimal angle $\alpha > 0$ such that for any $h > 0$ and any $T_i \in \mathcal{T}_h$ one has $\alpha_i \geqq \alpha$ [11].

We denote by S_i the segments on Γ_∞^h given by the edges of the boundary triangulations T_i of $\mathcal{T}_h$. By $\{S_h\}_{h>0}$ with $S_h := \bigcup_{i\in B} S_i$, where B is a finite subset of the natural numbers $\mathbb{N}$. We assume that the triangulation Ω_h is chosen such that the corresponding family $\{S_h\}_{h>0}$ guarantees the validity of an inverse assumption. This implies inverse estimates [51], [52]. For all further considerations, the parameter h will stand for the maximum diameter of all triangles $T_i \in \mathcal{T}_h$. Let $C^0(\bar{\Omega}_h)$ denote the set of all continuous functions on Ω_h, having one-sided limits on the slit Σ and $\partial\Omega_h$, respectively. For the discretizaton of (2.46) we introduce the following finite-dimensional spaces on the polygonal domains Ω_h,

$$\begin{aligned}\tilde{V}_h := \{\tilde{v}_h \in C^0(\bar{\Omega}_h) |\ &\tilde{v}_{h|T_i} \text{ is linear on every } T_i \in \mathcal{T}_h \text{ and} \\ &\tilde{v}_h^+ - \tilde{v}_h^- = \beta \text{ on } \Sigma \text{ with any } \beta \in \mathbb{R}\},\end{aligned} \tag{2.49}$$

$$\tilde{V}_h^0 := \{\tilde{v}_h \in \tilde{V}_h |\ \tilde{v}_h^+ - \tilde{v}_h^- = 0 \quad \text{on } \Sigma\}, \tag{2.50}$$

$$\tilde{H}_h := \{\tilde{\psi}_h \in Ł_2(\Gamma_\infty^h) | \tilde{\psi}_{h|S_i} \text{ is constant on every } S_i \in S_h \text{ and } \langle\tilde{\psi}_h, 1\rangle_h = 0\}, \tag{2.51}$$

and the set of admissible finite elements

$$\tilde{K}_{s_0} := \{\tilde{v}_h \in \tilde{V}_h |\ |\nabla\tilde{v}_h|^2 \leqslant s_0\}. \tag{2.52}$$

Here we use the notation

$$\langle\phi, \psi\rangle_h := \int_{\Gamma_\infty^h} \phi(s)\psi(s)ds \tag{2.53}$$

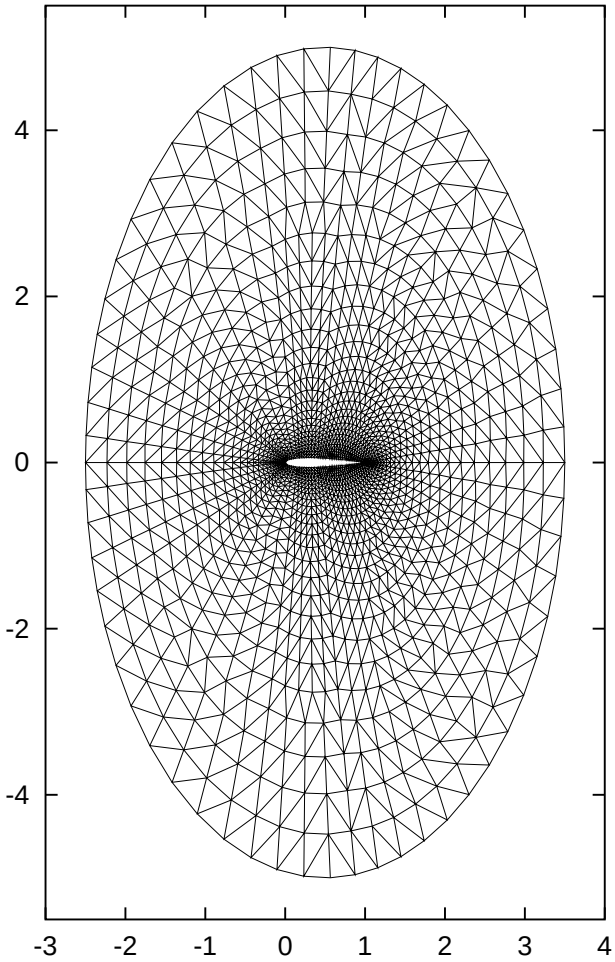

Figure 2: The finite element discretization for Ω.

for the L_2-scalar product on Γ_∞^h.

For the following, we need an approximate kernel K_h which is defined as in (2.38) where $\vec{n}(\vec{y})$ is to be replaced by $\vec{n}_h(\vec{y})$, the linear interpolant of the normal vectors to Γ_∞ at the vertices of Γ_∞^h. The associated operator will be denoted by $\mathcal{K}_h$. We further define the discrete forms

$$\begin{aligned}
a_h(\tilde{u}|\tilde{v},\tilde{\omega}) &:= \int_{\Omega_h} \varrho(|\nabla\tilde{u}|^2)\nabla\tilde{v}\cdot\nabla\tilde{\omega}dx,\\
\tilde{b}_h(\tilde{\lambda},\tilde{\psi}) &:= \langle\mathcal{V}\tilde{\lambda},\tilde{\psi}\rangle_h,\\
\tilde{d}_h(\tilde{u},\tilde{\psi}) &:= \langle\mathcal{K}_h\tilde{u},\tilde{\psi}\rangle_h,\\
\tilde{l}_1^h(\tilde{v},\beta) &:= \varrho_\infty\langle\nabla\Psi(\cdot,\beta)\cdot\vec{n}_h,\tilde{v}\rangle_h,\\
\tilde{l}_2^h(\tilde{\psi},\beta) &:= \langle(\mathcal{I}-\mathcal{K}_h)\Psi(\cdot,\beta),\tilde{\psi}\rangle_h.
\end{aligned} \tag{2.54}$$

Now the discrete analogue of problem (2.46) reads as follows:
The discrete variational problem

Find $(\tilde{u}_h, \tilde{\lambda}_h, \beta_h) \in \tilde{K}_{s_0} \times \tilde{H}_h \times \mathbb{R}$ such that

$$\begin{aligned} &a_h(\tilde{u}_h|\tilde{u}_h, \tilde{v}_h) - \langle \tilde{\lambda}_h, \tilde{v}_h \rangle_h = \tilde{l}_1^h(\tilde{v}_h, \beta_h) \text{ for all } \tilde{v}_h \in \tilde{V}_h, \\ &\tilde{b}_h(\tilde{\lambda}_h, \tilde{\psi}_h) + \langle \tilde{u}_h, \tilde{\psi}_h \rangle_h - \tilde{d}_h(\tilde{u}_h, \tilde{\psi}_h) = \tilde{l}_2^h(\tilde{\psi}_h, \beta_h) \text{ for all } \tilde{\psi}_h \in \tilde{H}_h \end{aligned} \tag{2.55}$$

subject to $F(\beta_h) = 0$.

The probelm (2.55) leads to a system of nonlinear equations, where we have one unknown per node in the triangulation $\mathcal{T}_h$ of Ω_h, one unknown per segment S_i of the polygonal boundary Γ_∞ and the unknown circulation β_h.

2.5 The discrete minimization and computational algorithm

In this secton we consider the description of the discrete variational problem (2.55) as the discrete minimization problem. The underlying idea goes back to [22], and has since been further developed, see [2]. For transonic flow, the hyperbolic character of the supersonic region creates additional difficulties. As pointed out beforehand, we must take into account an additional selection principle. This will be done by a penalization due to [22]. To this end, we use the following functional $\mathcal{J}_h : \tilde{V}_h \cap \tilde{K}_{s_0} \to \mathbb{R}$

$$\mathcal{J}_h(\phi_h) := \begin{cases} \dfrac{1}{2}\displaystyle\int_{\Omega_h} |\nabla \xi_h(\phi_h)|^2 dx & \text{if globally } s_0 < \frac{2a_0^2}{\kappa+1} \text{(subsonic)}, \\ \dfrac{1}{2}\displaystyle\int_{\Omega_h} |\nabla \xi_h(\phi_h)|^2 dx + \mathcal{P}_h(\phi_h) & \text{for } s_0 < \frac{2a_0^2}{\kappa-1} \text{ (transonic)} \end{cases} \tag{2.56}$$

where the penalty functional $\mathcal{P}_h : \tilde{V}_h \cup \tilde{K}_{s_0} \to \mathbb{R}$ is given by

$$\mathcal{P}_h(\phi_h) := \frac{\mu}{2} \sum_{\substack{i=1 \\ p_i \notin \Sigma \cup \Gamma_\infty^h}}^{N} \frac{1}{A_i^\epsilon} \left(\left[- \int_{\Omega_h} \nabla \phi_h \cdot \nabla \omega_{h_i} dx - B \int_{\Omega_h} \omega_{h_i} dx \right]^+ \right)^2, \tag{2.57}$$

see [5]. By $[\cdot]^+$ we denote the nonnegative part of the quantity in brackets. Here, $\mu > 0$, $B > 0$ and $2 > \epsilon > 1$ are constants, which do not depend on h. These constants can be chosen according to numerical experiments depending on the specific profile and the travelling velocity $\vec{v}_\infty$. The function $\xi_h(\phi_h) \in V_h^0$ is the solution of the following state equation

$$\begin{aligned} &\int_{\Omega_h} \nabla \xi_h(\phi_h) \cdot \nabla v_h dx \\ &\qquad = a_h(\phi_h | \phi_h, v_h) - \langle \lambda_h(\phi_h, \beta), v_h \rangle_h - \tilde{l}_1^h(v_h, \beta_h) \quad \text{for all } v_h \in \tilde{V}_h^0. \end{aligned} \tag{2.58}$$

This state equation is the finite element approximation of the Neumann problem for the Poisson equation with given Neumann data on Γ_p and on Γ_∞ where λ_h is given. On the other hand, $\lambda_h(\phi_h) \in \tilde{H}_h$ is to be determined by the Galerkin discretization of the boundary integral equation

$$\tilde{b}_h(\lambda_h(\phi_h, \beta_h), \psi_h) = \tilde{l}_2^h(\psi_h, \beta_h) - \langle \phi_h, \psi_h \rangle_h + \tilde{d}_h(\phi_h, \psi_h) \text{ for all } \psi_h \in \tilde{H}_h. \tag{2.59}$$

Instead of solving the discrete equations (2.55), we will now solve the following:

Discrete minimization problem

Find $(u_h, \lambda_h, \beta_h) \in \tilde{K}_{s_0} \times \tilde{H}_h \times I$ such that

$$(\mathcal{P}) \qquad \mathcal{J}_h(u_h) := \min_{\phi_h \in \tilde{K}_{s_0}} \mathcal{J}_h(\phi_h) \tag{2.60}$$

under the entropy condition and $F(\beta_h) = 0$ where F is given by (2.21), $\mathcal{J}_h(\phi_h)$ is defined via (2.56) and $I \subset \mathbb{R}$ is an appropriately fixed finite interval.

Since β_h is the circulation of u_h, it is sought only in a bounded interval I. The solution of problem (2.60) subject to $F(\beta_h) = 0$, (2.58) and (2.59) exists, because we minimize a differentiable functional over a bounded, convex and nonempty subset of a finite-dimensional space. The nonemptyness is due to the fact that the zero function lies in $\tilde{K}_{s_0}$ and satisfies $F(0) = 0$. The solution $u_h \in \tilde{K}_{s_0}$ is not necessarily unique, nevertheless, any solution u_h defines a corresponding flux $\lambda_h(u_h) \in \tilde{H}_h$ as the unique solution of (2.59). Thus we may assume for a given sequence of meshsizes the existence of a sequence $\{(u_h, \lambda_h, \beta_h)\}_{h>0}$, where $u_h \in \tilde{K}_{s_0}$ is a solution (2.60) and $\lambda_h \in \tilde{H}_h$ is the corresponding solution of (2.59) with the corresponding β_h. If $\mathcal{J}_h(u_h) = 0$, then $(u_h, \lambda_h, \beta_h)$ is a solution of (2.55). If we assume that the original problem has a solution (which is still open problem), then in [5] the convergence of the discrete minimization problem to the original problem was shown.

The discrete minimization problem (2.60) can be sloved by a Polak-Ribiére type conjugate gradient algorithm, which takes into account the constraint $F(\beta) = 0$ and the weak coupling equation (2.59).

The computational algorithm

$\triangle$ Starting Value

For an appropriate initial approximation we choose the solution of the corresponding incompressible, irrotational flow problem, i.e., by solving the Laplace equation. We determine $\phi_h^0 \in V_h$ and $\beta^0 \in \mathbb{R}$ as the solution of the variational problem,

$$\int_{\Omega_h} \nabla\phi_h^0 \cdot \nabla\psi_h dx = \int_{\Gamma_\infty^h} \vec{V}_\infty \cdot \vec{n}_\infty \psi_h ds \qquad \forall\psi_h \in \tilde{V}_h^0$$
$$\text{subject to } F(\beta) = 0. \tag{2.61}$$

The problem (2.61) and the corresponding continuous problem have a unique solution as is well known from conformal mappings, see [15].

Then we define $\lambda_h^0 \in \tilde{H}_h$ as the solution of

$$\tilde{b}_h(\lambda_h^0, \eta_h) = \tilde{l}_2^h(\eta_h, \beta^0) - \langle\phi_h^0, \eta_h\rangle_h + \tilde{d}_h(\phi_h^0, \eta_h) \text{ for all } \eta_h \in \tilde{H}_h.$$

The above boundary integral equation can be solved by the Galerkin-collocation method for boundary integral equations of the first kind [33].

$\triangle$ Initial Step

Now we solve the variational equation for $g_h^0 \in \tilde{V}_h^0$, namely

$$\int_{\Omega_h} \nabla g_h^0 \cdot \nabla\psi_h dx = \langle\acute{\mathcal{J}}_h(\phi_h^0), \psi_h\rangle \quad \forall\psi_h \in \tilde{V}_h^0, \tag{2.62}$$

where

$$\langle \acute{\mathcal{J}}_h(\phi_h^0), \psi_h \rangle := \int_{\Omega_h} \varrho(|\nabla \phi_h^0|^2) \nabla \xi_h \cdot \nabla \psi_h dx$$

$$+ \int_{\Omega_h} \acute{\varrho}(|\nabla \phi_h^0)|^2)(\nabla \phi_h^0 \cdot \nabla \xi_h)(\nabla \phi_h^0 \cdot \nabla \psi_h) dx \tag{2.63}$$

$$+ \mu \sum_{i=1}^{N} \frac{3}{A_i} \left(\int_{\Omega_h} \nabla \phi_h^0 \cdot \nabla \omega_{h_i} dx - B \frac{A_i}{3} \right)^+ \left(\int_{\Omega_h} \nabla \psi_h \cdot \nabla \omega_{h_i} \right) dx,$$

and where $\xi_h := \xi_h(\phi_h^0, \lambda_h^0) \in \tilde{V}_h^0$ is defined as the FEM-soultion of the variational Possion equation

$$\int_{\Omega_h} \nabla \xi_h^0 \cdot \nabla \eta_h dx = a_h(\phi_h^0 | \phi_h^0, \eta_h) - \langle \lambda_h^0, \eta_h \rangle - \tilde{l}_1^h(\eta_h, \beta^0), \text{ for all } \eta_h \in \tilde{V}_h^0.$$

Finally we set

$$z_h^0 = g_h^0. \tag{2.64}$$

Iteration Scheme

• Outer iteration:

For $m = 0$ we take the starting value as λ_h^0 :

• Inner iteration: Assume now $\phi_h^n, \lambda_h^m, g_h^n, z_h^n$ are known for $n \geqslant 0$. Then we compute $\phi_h^{n+1}, \lambda_h^{m+1}, g_h^{n+1}, z_h^{n+1}$ as follows:

Step 1. Define $\mathcal{J}_h(\phi_h^n)$ using the solution $\xi_h^n := \xi_h^n(\phi_h^n, \beta^n) \in \tilde{V}_h^0$ of the Possion problem

$$\int_{\Omega_h} \nabla \xi_h^n \cdot \nabla \eta_h dx = a_h(\phi_h^n | \phi_h^n, \eta_h) - \langle \lambda_h^m, \eta_h \rangle_h - \tilde{l}_h^h(\eta_h, \beta^n), \text{for all } \eta_h \in \tilde{V}_h^0.$$

Then we solve the one-dimensional minimization problem (line search):

Find $\tilde{\lambda} \leqslant 0$ as the solution of the equation

$$\mathcal{J}_h(\phi_h^n - \tilde{\lambda} z_h^n) \leqslant \mathcal{J}_h(\phi_h^n - \lambda z_h^n) \quad \text{for all } \lambda \leqslant 0 \tag{2.65}$$

and set

$$\tilde{\phi}_h^{n+1} = \phi_h^n - \tilde{\lambda} z_h^n. \tag{2.66}$$

Step 2. In this step we incorporate the constraint $F(\beta) = 0$ and compute the new circulation β^{n+1} as follows.

Define a modification of $\tilde{\phi}_h^{n+1}$

$$\tilde{\phi}_h^{n+1} \mapsto \bar{\phi}_h^{n+1} \in \tilde{V}_h \tag{2.67}$$

s.t. $\bar{\phi}_h^{n+1}$ satisfies the Kutta-Joukowski condition at TE in the form

$$F(\bar{\beta}^{n+1}) = |\nabla \phi_h^{n+1}|_{T^+}|^2 - |\nabla \phi_h^{n+1}|_{T^-}|^2 = 0 \tag{2.68}$$

where T^+ and T^- denote the triangles adjacent to TE from below and above, respectively. For this modification, the main idea is, that we only modify $\tilde{\phi}_h^{n+1}$ at the points P_j^+ and $P_j^-, j = 1, ..., L$ along the slit Σ.

Hence the new function $\bar{\phi}_h^{n+1}$ will differ from $\tilde{\phi}_h^{n+1}$ only at the $2L$ points $P_j^+, P_j^-, j = 1, ..., L$ on Σ.

We now describe the modification of $\tilde{\phi}_h^{n+1}$ in detail. For $P_i \in \Omega \backslash \Sigma$ we put

$$\bar{\phi}_h^{n+1}(P_i) = \tilde{\phi}_h^{n+1}(P_i) \quad P_i \in \Omega \backslash \Sigma. \tag{2.69}$$

At the point $P_i = TE \in \Sigma$ we $\bar{\phi}_h^{n+1}(P_1^-) := \tilde{\phi}_h^{n+1}(P_i^-)$, we compute $\bar{\phi}_h^{n+1}(P_1^+)$ and β by the following two equations

$$\begin{aligned} F(\bar{\beta}^{n+1}) = |\nabla \bar{\phi}_h^{n+1}|_{T^+}|^2 - |\nabla \bar{\phi}_h^{n+1}|_{T^-}|^2 = 0, \\ \bar{\beta}^{n+1} = \bar{\phi}_h^{n+1}(P_1^+) - \bar{\phi}_h^{n+1}(P_1^-). \end{aligned} \tag{2.70}$$

The values $\bar{\phi}_h^{n+1}(P_j^+), \bar{\phi}_h^{n+1}(P_j^-), j = 2, ..., L$ at the remaining points on Σ are determined by the condition $\bar{\phi}_h^{n+1} \in \tilde{V}_h$, which means that $\bar{\phi}_h^{n+1}$ will have the constant jump of strength $\bar{\beta}^{n+1}$ and continuous normal derivatives along Σ. This yields the set of equations

$$\begin{aligned} &\bar{\phi}_h^{n+1}(P_j^+) - \bar{\phi}_h^{n+1}(P_j^-) = \bar{\beta}^{n+1} \\ &\qquad\qquad\qquad\qquad j = 2, ..., L \qquad \text{on } \Sigma \\ &\partial_n \bar{\phi}_h^{n+1}(P_j^+) - \partial_n \bar{\phi}_h^{n+1}(P_j^-) = 0, \end{aligned} \tag{2.71}$$

which leads to a system of $2(L-1)$ linear equations for the $2(L-1)$ unknowns $\bar{\phi}_h^{n+1}(P_j^+), \bar{\phi}_h^{n+1}(P_j^-), j = 2, ..., L$.

For the time being, this procedure could not yet be rigorously justified. Numerical experiments did not always show satisfactory convergence. Therefore, we use a relaxation technique by taking

$$\begin{aligned} \phi_h^{n+1} &:= \omega \bar{\phi}_h^{n+1} + (1-\omega)\tilde{\phi}_h^{n+1} \\ &\qquad\qquad\qquad \text{with } \omega \in (0.1], \\ \beta^{n+1} &:= \omega \bar{\beta}^{n+1} + (1-\omega)\beta^n \end{aligned} \tag{2.72}$$

Step 3. We compute the gradient $g_h^{n+1} \in \tilde{V}_h^0$ of the new descent direction as the solution of the variational problem

$$\int_{\Omega_h} \nabla g_h^{n+1} \cdot \nabla \psi_h dx = \langle \acute{\mathcal{J}}_h(\phi_h^{n+1}), \psi_h \rangle \quad \forall \psi_h \in \tilde{V}_h^0. \tag{2.73}$$

Then the new descent direction $z_h^{n+1} \in \tilde{V}_h^0$ is given by

$$z_h^{n+1} = g_h^{n+1} + \gamma^{n+1} z_h^n \tag{2.74}$$

where

$$\gamma^{n+1} = \frac{\int_{\Omega_h} \nabla g_h^{n+1} \cdot \nabla (g_h^{n+1} - g_h^n) dx}{\int_{\Omega_h} |\nabla g_h^n|^2 dx}. \tag{2.75}$$

The whole iteration procedure, starting from Step 1, will be repeated until the residuals of the solution reach a minimum.

• End of inner iteration

Then, we take λ_h^{m+1} by solving the discrete boundary integral equation

$$\tilde{b}_h(\lambda_h^{m+1}, \eta_h) = \tilde{l}_2^h(\eta_h, \beta^m) - \langle \phi_h^m, \eta_h \rangle_h + \tilde{d}_h(\phi_h^m, \eta_h), \text{ for all } \eta_h \in \tilde{H}_h.$$

For $\lambda_h^{m+1} \in \tilde{H}_h$ repeat the outer iteration until $\|\lambda_h^{m+1} - \lambda_h^m\|_{L^2(\Gamma_\infty)}$ is smaller than a given tolerance.

End of outer iteration.

2.6 The computational results for transonic flow

In this section we show the computational results for the transonic fluid flow around NACA0012 and NACA2412 airfoils. In each computations we choose the exterior boundary Γ_∞ of the problem as an ellipse (see Figure 2). A grid with 2630 nodepoints, 5036 triangles and 164 nodepoints on the profile was used here. Depending on the free stream Mach number and angle of attack, the modified conjugate gradient algorithm needs 300 to 500 iterations for convergence of the minimization functional. The computational time lies between 60 and 90 seconds. Here we concentrated on getting the computational results of the state equation necessary for the shape optimization of the transonic airfoil. Therefore what we are interested in are the following points:

• Choice of the parameters $B \in \mathbb{R}$, $\mu > 0$ and their dependence on the meshsize, initial velocity, angle of attack and the shape of the profile.

• Influence of the penalty term $\mathcal{P}_h(\phi_h)$ in the domain.

• The quantities on the profile, e.g. lift, pressure, drag coefficients and Mach number.

We performed the numerical experiments with a free stream Mach number $M_\infty = 0.70, 0.75$ and the angles of attack $\alpha = 0, 1.0, 2.0, 2.5$ for NACA0012 and NACA2412 profiles.

△ The numerical experiments for NACA0012

Here the Mach number and pressure coefficient ditribution on the profile NACA0012 with $M_\infty = 0.70$ is shown for various angles of attack.

• $M_\infty = 0.70, \quad \alpha = 0°, \quad \mu = 5 \cdot 10^{-6}$

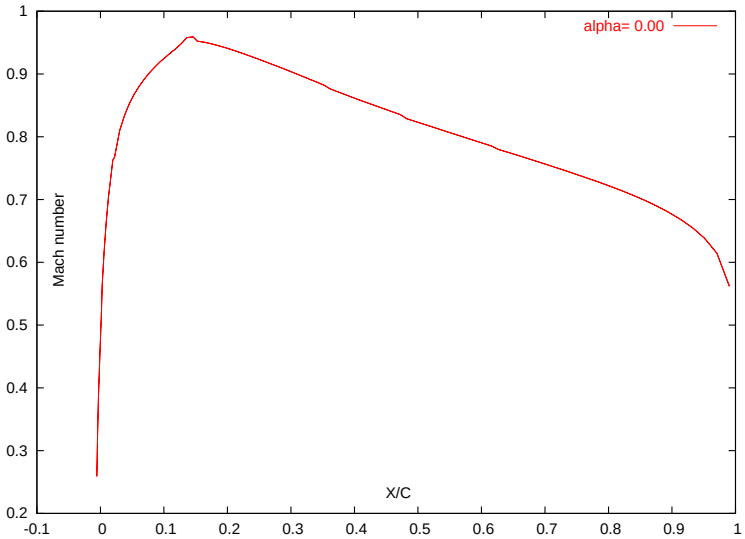

Figure 3: The Mach number distribution for $M_\infty = 0.70, \quad \alpha = 0°$.

For this configration we obtain a transonic flow solution without shock and due to the symmetry of the profile, the values of potentials ϕ^+ and ϕ^- at the trailing edge almost coincide (see Figure 3).

- $M_\infty = 0.70, \quad \alpha = 1^\circ, \quad \mu = 5 \cdot 10^{-6}$.

In this case the situation is quite different from the previous case. We can see that there occurs a shock at the front part of the profile and the lift is non-zero (see Figure 4).

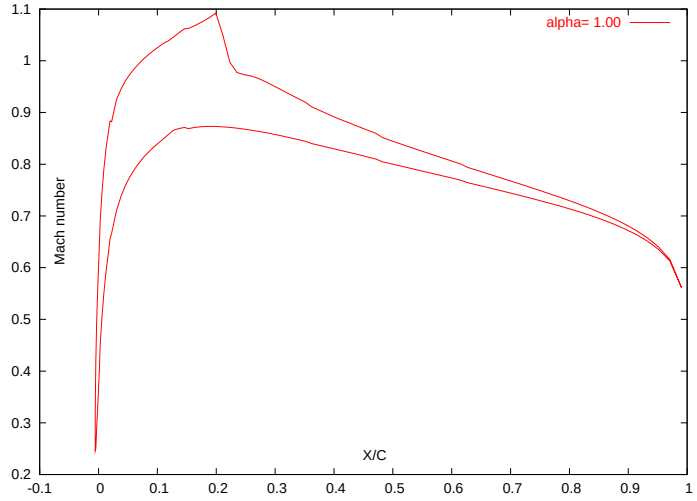

Figure 4: The Mach number distribution for $M_\infty = 0.70, \quad \alpha = 1^\circ$.

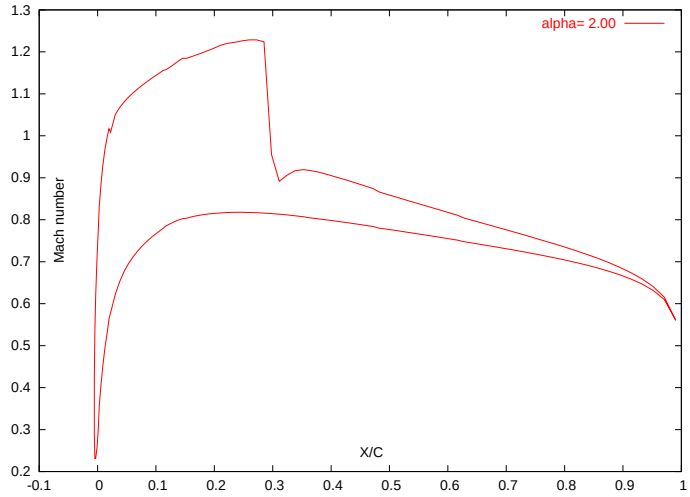

Figure 5: The Mach number distribution for $M_\infty = 0.70, \quad \alpha = 2^\circ$.

- $M_\infty = 0.70, \quad \alpha = 2°, 2.5°, \quad \mu = 5 \cdot 10^{-6}$

As we can see from the figures, there exist shocks and this position moves to back part of the profile as the angle of attack increases. See figures 5, 6.

Collecting the results for NACA0012 with the free stream Mach number $M_\infty = 0.70$, we can see more considerable differences for various angles of atack (see Figure 7).

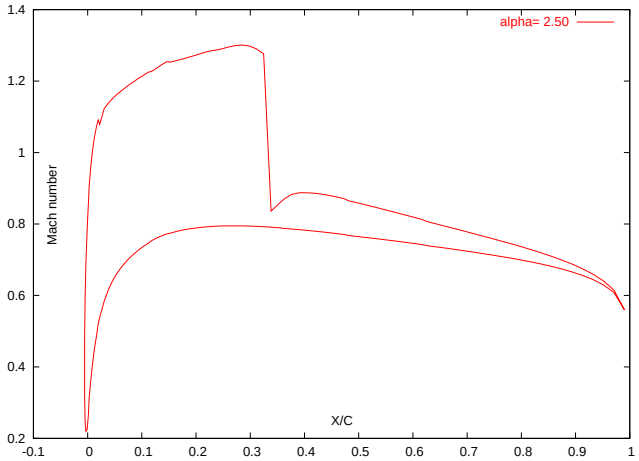

Figure 6: The Mach number distribution for $M_\infty = 0.70, \quad \alpha = 2.5°$.

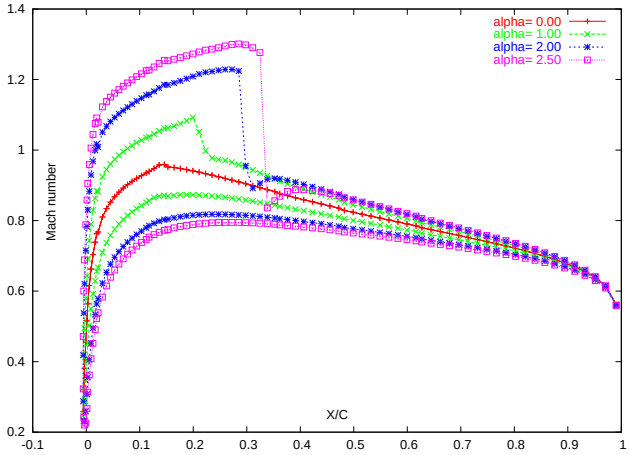

Figure 7: The Mach number distributions for $M_\infty = 0.70$.

- $M_\infty = 0.75, \quad \alpha = 0°, 1°, 2°, 2.5°, \quad \mu = 5 \cdot 10^{-6}$.

We obtain similiar results for $M_\infty = 0.75$. But, in this case even if the angle of attack is zero, there exists a compressive shock around the profile. See figures 8, 9, 10, 11, 12.

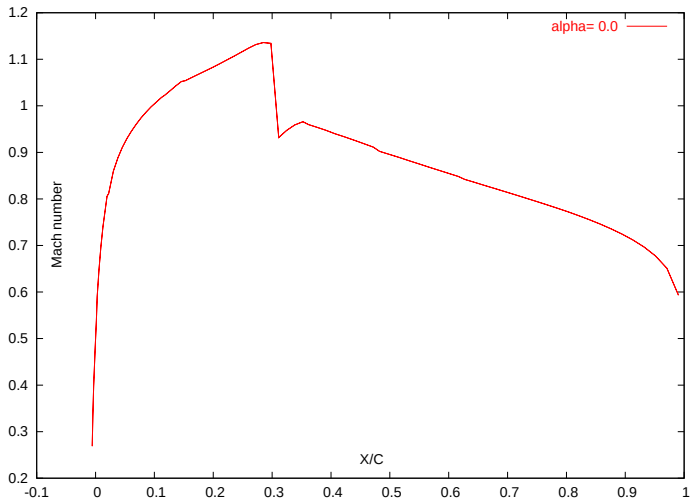

Figure 8: The Mach number distribution for $M_\infty = 0.75, \quad \alpha = 0°$.

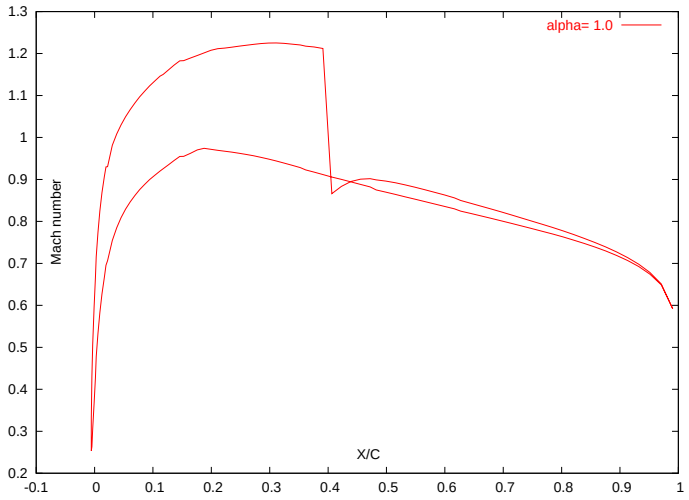

Figure 9: The Mach number distribution for $M_\infty = 0.75, \quad \alpha = 1°$.

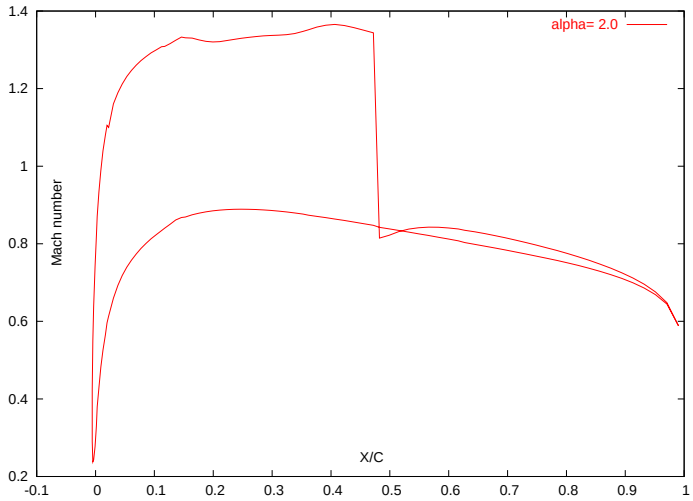

Figure 10: The Mach number distribution for $M_\infty = 0.75, \quad \alpha = 2°$.

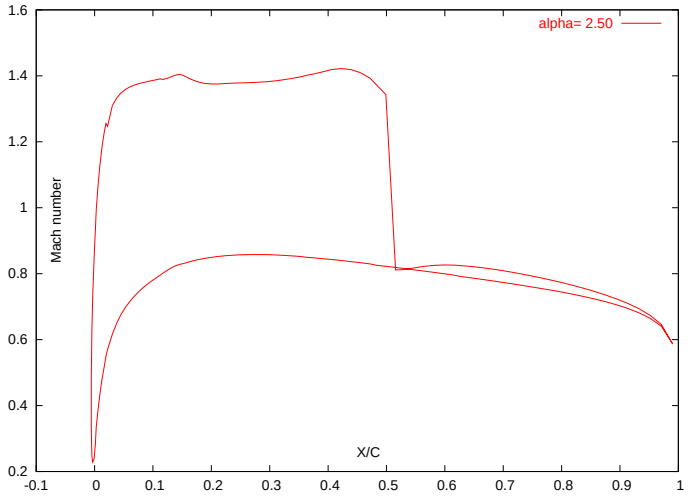

Figure 11: The Mach number distribution for $M_\infty = 0.75, \quad \alpha = 2.5°$.

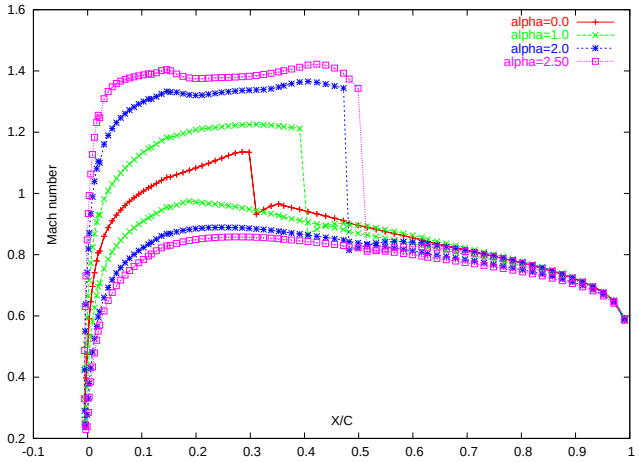

Figure 12: The Mach number distribution for $M_\infty = 0.75$.

△ The numerical experiments for NACA2412

The NACA2412 airfoil is an asymmetric profile. Therefore even if the angle of attack is zero, the lift exists and we must be more careful with the computation comparison with the previous case. For the NACA2412 airfoil we take μ between $1 \cdot 10^{-6}$ and $3 \cdot 10^{-6}$. For the free sream Mach number $M_\infty = 0.70$ the position of the shock lies around the middle of the profile, whereas for $M_\infty = 0.75$, shocks exist at the position close to the trailing edge (see Figures 13, 14).

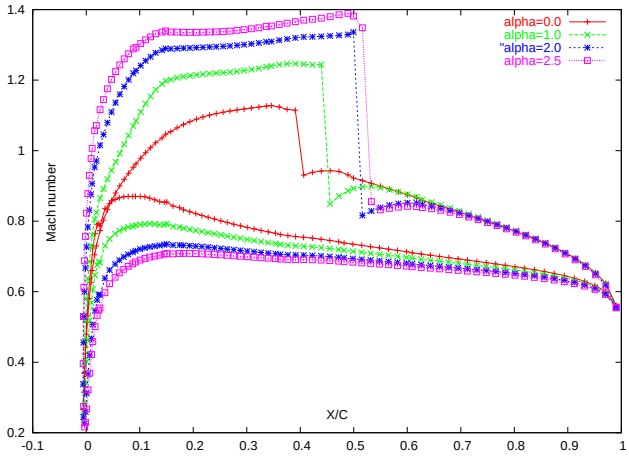

Figure 13: The Mach number distribution for $M_\infty = 0.70$.

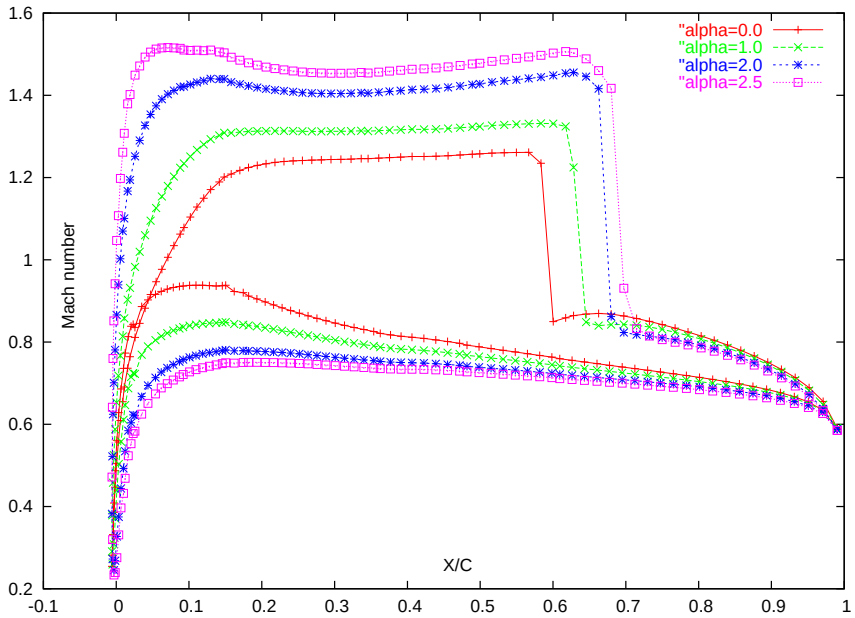

Figure 14: The Mach number distribution for $M_\infty = 0.75$.

△ Comparison experiments

We compare our computational results with the results of the Euler code.

• Comparison of pressure coffeficients

For comparison we performed numerical experiments for the NACA2412 airfoil with the free stream Mach number $M_\infty = 0.70$, angles of attack $\alpha = 0.0°$, $1.0°$ for our code and an Euler code, respectively. From these comparisons we see that the shocks lie at similiar positions and the shapes of the graphs for the pressure coefficients are close to each other(see Figure 15).

• Comparison of lift coefficients

For the comparison of the lift coefficients we derived numerical results changing the angle of attack from $-2°$ to $2.5°$. As can be seen from Figure 16, the vlaues of the lift coefficients obtained with the two codes are quite similiar in the interval $[-2°, 1°]$.

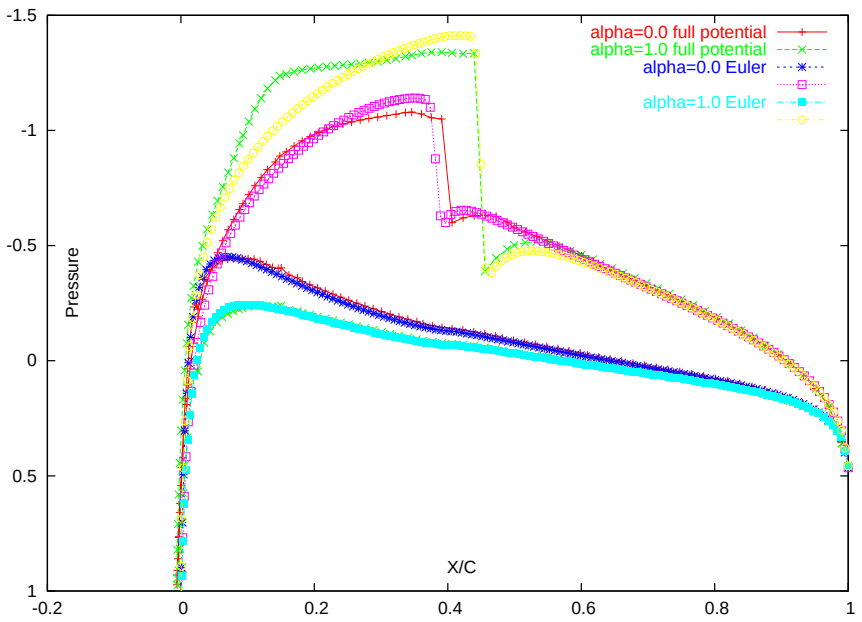

Figure 15: The comparison of the pressure coefficient distributions for the full potential equation and the Euler equation.

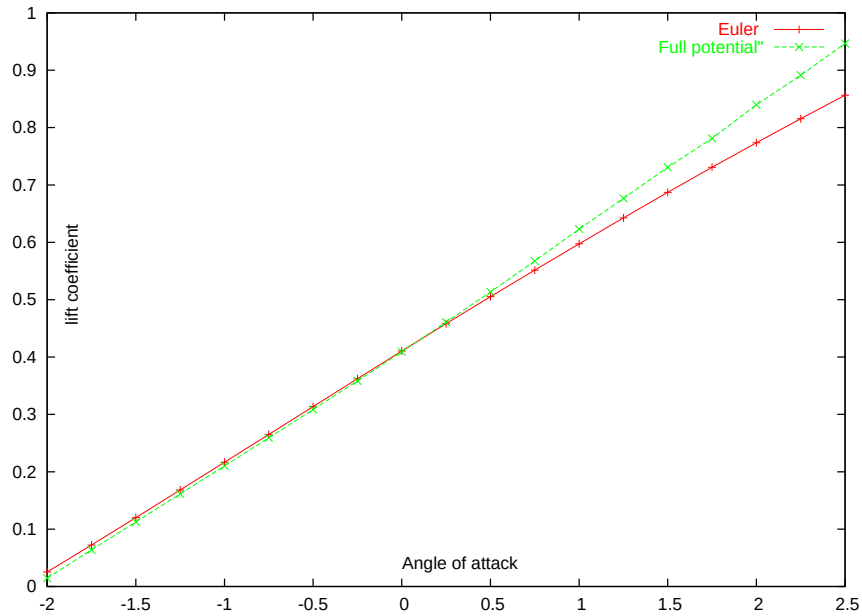

Figure 16: The comparison of the lift coefficients for the full potential equation and the Euler equation.

2.7 The convergence of the approximation for the discrete minimization problem

In this section we approximate the penalty term $\mathcal{P}_h(\phi_h)$ of (2.57) by the sequence of the second order differentiable functions, prove the convergence of this sequence, and give some numerical results showing this convergence.

Approximation of the discrete minimization problem

As mentioned in the previous section, the numerical experiments give us good results available for employing the shape optimization. However, in order to construct the adjoint state equation for finding the shape gradient it is necessary to find the second order derivative with respect to the velocity potential of the penalty term $\mathcal{P}_h(\phi_h)$ of (2.57), but this term is only one time differentiable, not twice. To this end we consider the following approximating function depending on some parameter $\delta > 0$ [39]:

$$\gamma_\delta(y) := \begin{cases} y - \dfrac{\delta}{2} & \text{for} \quad y > \delta, \\ \dfrac{1}{2\delta} y^2 & \text{for} \quad 0 < y \leqslant \delta, \\ 0 & \text{for} \quad y \leqslant 0. \end{cases} \tag{2.76}$$

The function $(\gamma_\delta(y))^2$ is two times differentiable and $\{\gamma_\delta\}_{\delta>0}$ describes the approximation of the non-negative part of y. Therefore, we can use this sequence of functions $\{\gamma_\delta\}_{\delta>0}$ as the second order differentiable approximation of the penalty term $\mathcal{P}_h(\phi_h)$. Based on this idea, we define the approximation for the discrete minimization problem (2.60):

$$(\mathcal{P}_\delta) \qquad \mathcal{J}_h^\delta(u_h^\delta) := \min_{\phi_h^\delta \in \tilde{K}_{s_0}} \mathcal{J}_h^\delta(\phi_h^\delta), \tag{2.77}$$

where

$$\mathcal{J}_h^\delta(\phi_h) := \begin{cases} \dfrac{1}{2}\displaystyle\int_{\Omega_h} |\nabla \xi_h(\phi_h)|^2 dx & \text{for } s_0 < \frac{2a_0^2}{\kappa+1} \text{ (subsonic)}, \\ \dfrac{1}{2}\displaystyle\int_{\Omega_h} |\nabla \xi_h(\phi_h)|^2 dx + \mathcal{P}_h^\delta(\phi_h) & \text{for } s_0 < \frac{2a_0^2}{\kappa-1} \text{ (transonic)} \end{cases},$$

and

$$\mathcal{P}_h^\delta(\phi_h) := \frac{\mu}{2} \sum_{\substack{i=1 \\ p_i \notin \Sigma \cup \Gamma_\infty^h}}^{N} \frac{1}{A_i^\epsilon} [\gamma_\delta(-\int_{\Omega_h} \nabla \phi_h \cdot \nabla \omega_{h_i} dx - B \int_{\Omega_h} \omega_{h_i} dx)]^2$$

.

Using

$$\gamma_\delta(y) < y < C_\delta \gamma_\delta(y),$$

we obtain the convergence of a sequence of solutions $\{u_h^\delta\}_{\delta>0}$ of problem $(\mathcal{P}_\delta)$.

Theorem 2.2 *Suppose that the following assumptions hold:*
(a) Let the family of triangulations be quasi-uniform.
(b) The problem (2.46) *has exactly one solution* $(u, \lambda, \beta) \in (V \cap K_{s_0}) \times H \times I$*, which satisfies the entropy condition.*
(c) The solution of (2.46) *satisfies the subsonic flow condition* (2.47) *near the trailing edge.*

Then there exists a constant $\tilde{s}_0 \geqslant s_0$ *such that a sequence of solutions* $\{\tilde{u}_h^\delta, \tilde{\lambda}_h^\delta, \beta_h^\delta\}_{h>0,\delta>0}$ *of the minimization problem*

$$\mathcal{J}_h^\delta(\tilde{u}_h^\delta) = \min_{\tilde{\phi}_h^\delta \in \tilde{V}_h \cap K_{s_0}} \mathcal{J}_h^\delta(\tilde{\phi}_h^\delta) \tag{2.78}$$

subject (2.58),(2.59) *and* $F(\beta_h^\delta) = 0$ *converges to the unique solution* (u, λ, β) *of the variational problem* (2.46)*.*

The proof of the theorem is analogous to [5].
Numerical experiments for the convergence

We tested the convergence of the approximation of the discrete minimization problem according to the following numerical experiments:

• NACA0012 airfoil, $M_\infty = 0.75$, $\alpha = 0.0$

The figure 17 shows the convergence of the Mach number distributions changing the value of δ between 0.01 and 0.005. The experiment shows that when $\delta \to 0$ it converges to the Mach number distribution for $\delta = 0$.

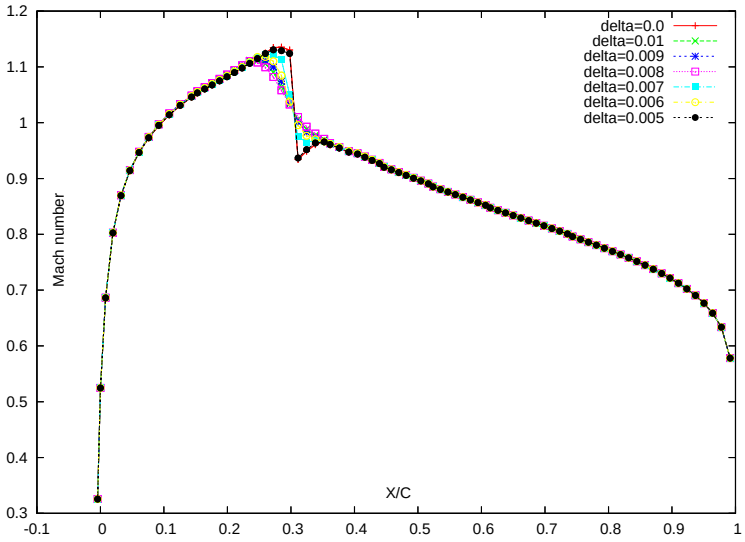

Figure 17: The convergence of Mach number distributions.

• NACA0012 airfoil, $M_\infty = 0.70$, $\alpha = 1.0$

value of δ	C_L	C_D	Circulation
0.01	0.192507702	0.00677341501	16.1640401
0.008	0.192553589	0.0067728598	16.1677017
0.006	0.192547271	0.00677120317	16.1690773
0.004	0.192584369	0.0067715508	16.1700317
0.001	0.192678616	0.00676993145	16.1769692
0.00	0.192712106	0.0067686394	16.17947

Table 1: Convergence of C_L, C_D,and circulation.

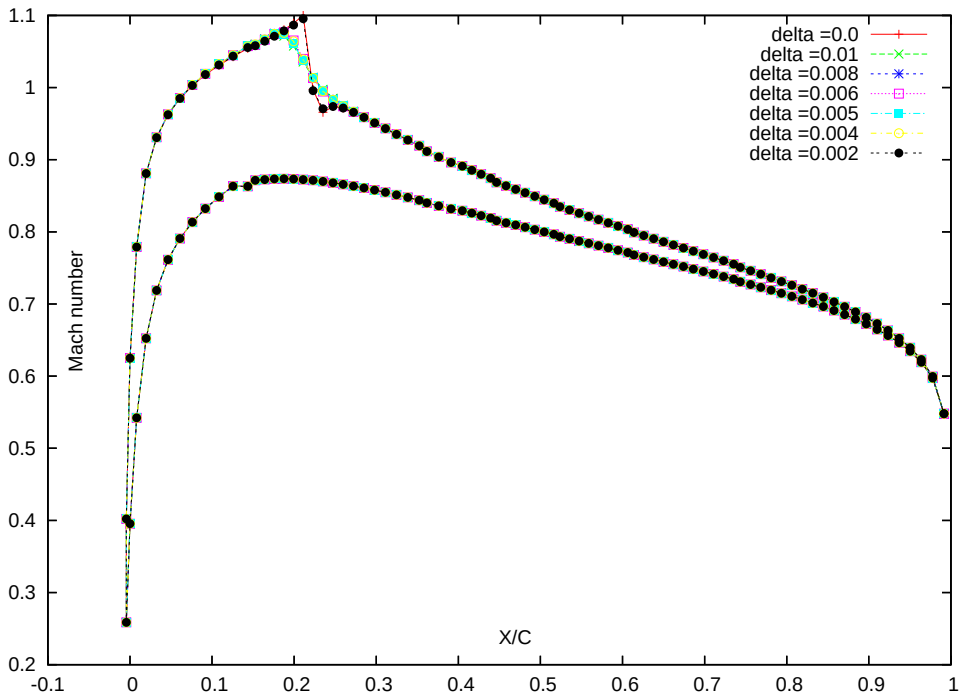

Figure 18: The convergence of Mach number distributions.

- NACA0012 airfoil, $M_\infty = 0.75$, $\alpha = 1.0$

value of δ	C_L	C_D	Circulation
0.1	0.228826215	0.00725066901	20.5707123
0.05	0.233967893	0.00710047961	20.9991766
0.01	0.238679289	0.00684817317	21.4078518
0.001	0.238257613	0.00686919622	21.3703833
0.0001	0.238092414	0.00687369905	21.3559521
0.00	0.237811319	0.00689032306	21.3311907

Table 2: Convergence of C_L, C_D,and circulation.

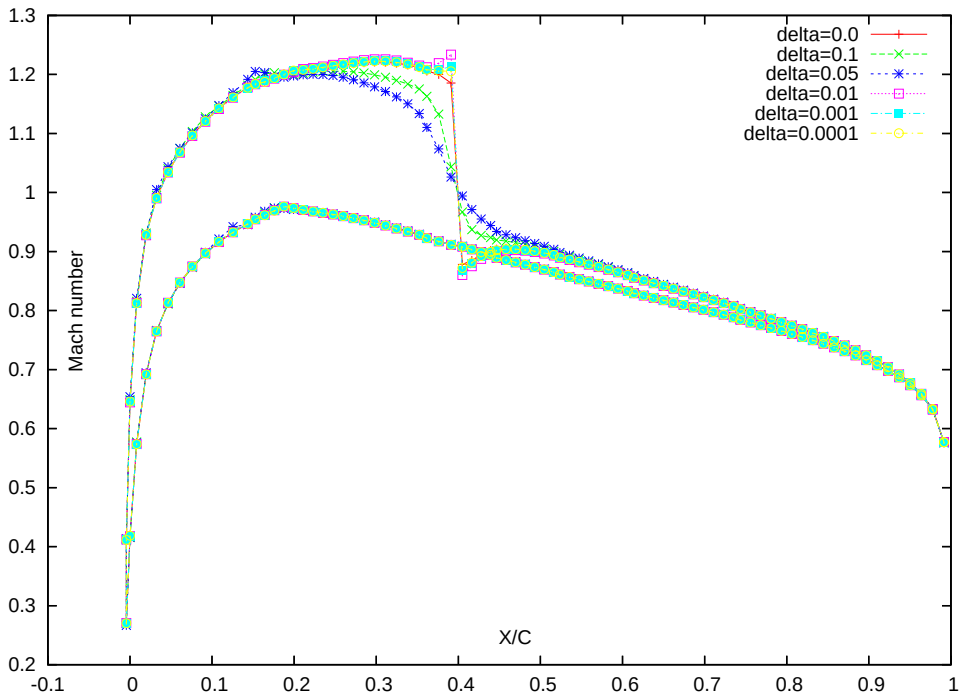

Figure 19: The convergence of Mach number distributions.

3 Shape optimization of a 2D transonic airfoil

In this section we set the shape optimization problem whose state equation is the full potential equation and parameterize the shape of the airfoil by some Bezier curves. Based on the shape sensitivity for the problem, we derive optimization algorithm and some computational results.

3.1 The motivation of the shape optimization

In this section we motivate the shape optimization based on the comparative examples of the lift and drag coefficients for NACA0012 and NACA2412 profiles with free stream Mach number $M_\infty = 0.70$.

Velocity and pressure are dependent on each other. According to Bernoulli's equation, increasing the velocity decreases the local pressure and vice versa. Thus the higher velocity on the upper airfoil side results in lower than ambient pressure whereas the pressure on the lower side is higher than the ambient pressure. As can be seen in the above numerical experiments, the pressure difference between the upper and lower surfaces is modified by changing the surface geometry and angle of attack. For aerodynamic shape optimization it is more convenient to express the phenomena around profile in terms of the dimensionless quantities, such as pressure, lift and drag coefficients.

The pressure coefficient is the ratio of the local pressure to the stagnation pressure:

$$C_P = \frac{P - P_\infty}{\frac{1}{2}\varrho \cdot v_\infty^2}. \tag{3.1}$$

The lift coefficient C_L and drag coefficient C_D can be expressed by the pressure coefficient C_P in the following way.

Let us denote C_z and C_x as follows:

$$C_z = \oint_{\Gamma_p} C_P \cdot d(\frac{x}{c}) \quad C_x = \oint_{\Gamma_p} C_P \cdot d(\frac{z}{c}),$$

where c is the chord length of a airfoil and Γ_p is a profile surface. Then the lift and drag coefficients can be written in terms of C_z and C_x:

$$C_L = C_z \cdot \cos\alpha - C_x \cdot \sin\alpha, \tag{3.2}$$

$$C_D = C_z \cdot \sin\alpha + C_x \cdot \cos\alpha, \tag{3.3}$$

where α is the angle of attack.

The below figure shows the graph of the lift and drag coefficients in dependence on the angle of attack for NACA0012 and NACA2412 profiles with free stream Mach number $M_\infty = 0.70$ (see Figure 20).

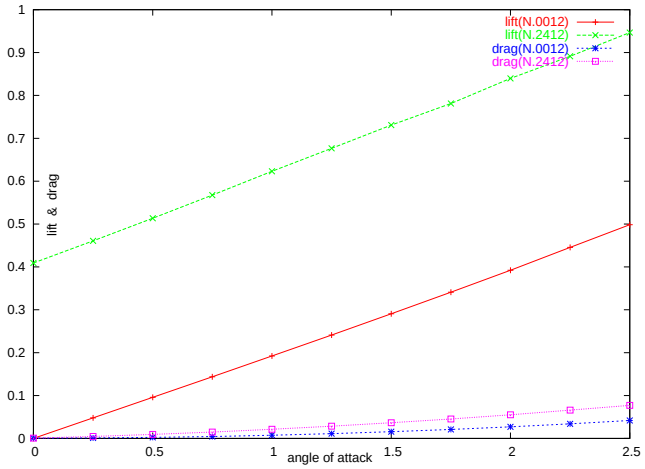

Figure 20: $C_L - C_D$ relationship for NACA0012, NACA2412 with $M_\infty = 0.70$.

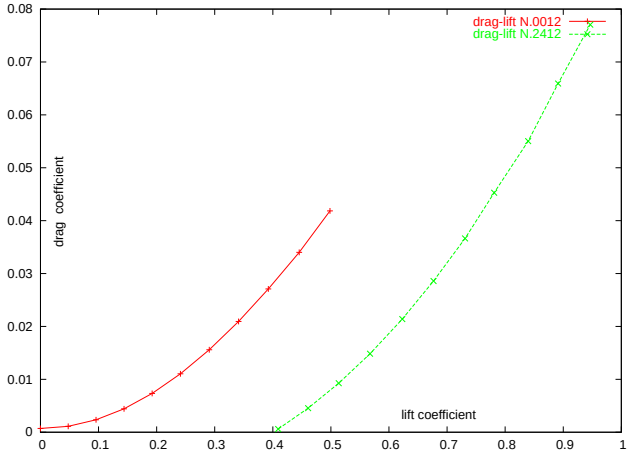

Figure 21: $C_L - C_D$ relationship for NACA0012 and NACA2412 $M_\infty = 0.70$.

The lift and drag coefficients for NACA2412 are bigger than those for NACA0012, and the difference between the lift coefficients for NACA0012 and NACA2412 are considerably bigger than the difference between the drag coefficients. We represent these relations in terms of a $C_D - C_L$ graph (see also Figures 21, 22 and 23).

According to these figures we can see that the NACA2412 seems to be better than NACA0012. In the same way we can compare the aerodynamic characteristics for various airfoils. Throughout these comparisons we have the desire to design the airfoil shape such that the lift is maximized and the drag is minimized.

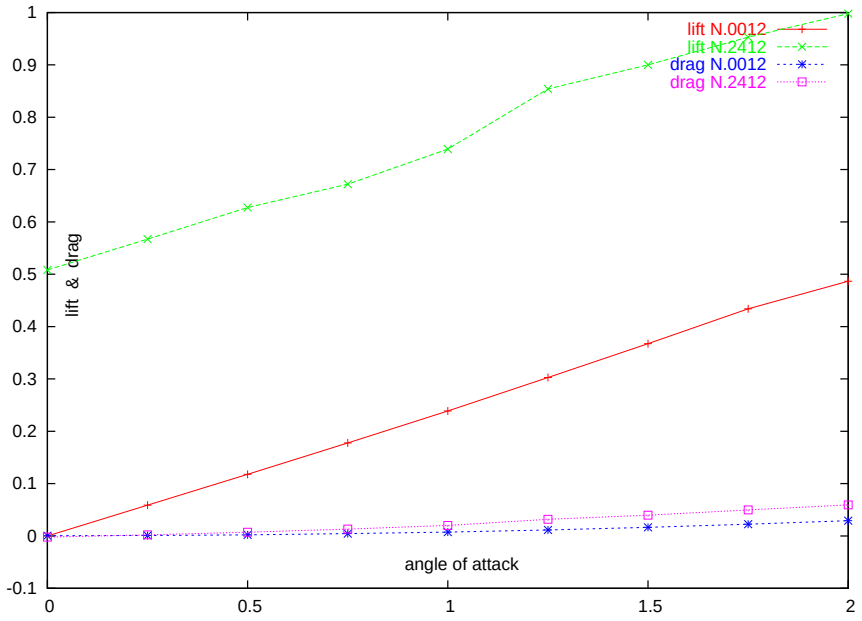

Figure 22: $C_L - C_D$ relationship for NACA0012 and NACA2412 $M_\infty = 0.75$.

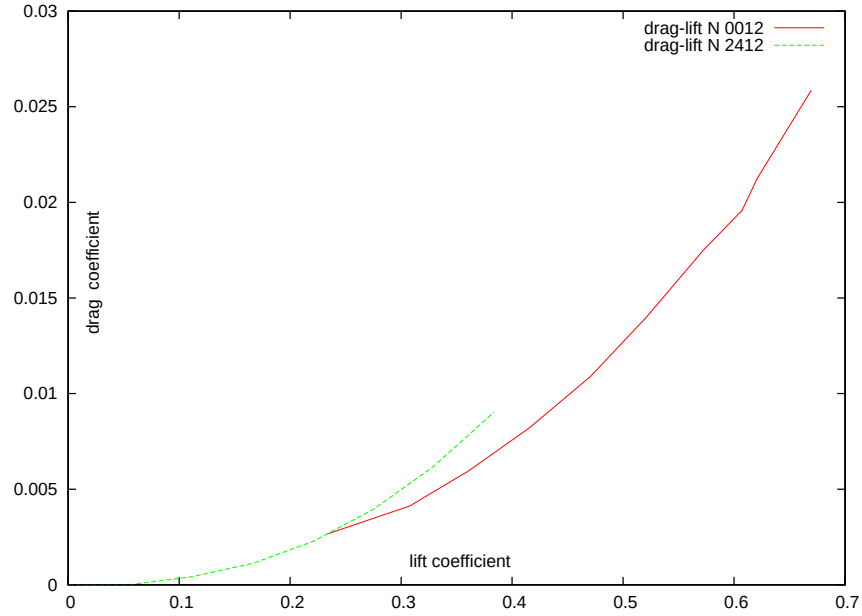

Figure 23: $C_L - C_D$ relationship for NACA0012 and NACA2412 $M_\infty = 0.75$.

3.2 The Bezier curve generation

The Bezier curves are widely used to obtain smooth surfaces in aerodynamic design. In this section we demonstrate the method how to reconstruct airfoils by Bezier curves.

A point on the Bezier curve is given by a parametric function of the following form:

$$\begin{cases} x_B(t) = \sum_{k=0}^{n} x_k B_n^k(t), \\ y_B(t) = \sum_{k=0}^{n} y_k B_n^k(t) \end{cases} \tag{3.4}$$

where $t \in [0,1]$ is a parameter varying continuously, $B_k^k(t) = C_n^k t^k (1-t)^{n-k} (k = 0, 1, ..., n)$ is a Bernstein polynomial of degree n, and , at this stage, (x_k, y_k) are coefficients. In these formulas, $x_B(t)$ and $y_B(t)$ are polynomials of degree n of the parameter t, and from an algebraic point of view, the introduction of the Bernstein basis neither enhance nor restricts this general statement.

The above formula (3.4) reads in vector form:

$$\mathbf{P}(t) = \sum_{k=0}^{n} \mathbf{P}_i B_{i,k}(t) \quad \text{for } t \in [0,1]. \tag{3.5}$$

The vector $\mathbf{P}_i$ represents the $k+1$ vertices of a characteristic polygon which are also called control points. A Bezier curve is completely specified if the vertices of the characteristic polygons are prescribed, and passes through the starting point $\mathbf{P}_0$ and the end point $\mathbf{P}_n$. The intermediate points $\mathbf{P}_1, \mathbf{P}_2, ..., \mathbf{P}_{n-1}$ need not to lie on the curve. If the starting point and the end point coincide, the curve is closed. In order to describe a more complex curve, we can use several Bezier curves of low degree polynomials instead of using only one Bezier curve of a high degree polynomial. For example in order to construct an airfoil it is possible to use two Bezier curves corresponding to the upper and lower surfaces, respectively.

We can rewrite Eq.(3.5) in matrix form as follows:

$$[P(t_i)] = [B_{i,n}][V_i]. \tag{3.6}$$

Here, $[B_{i,n}(t_i)]$ is the matrix associated with the Bernstein polynomial, and $[V_i]$ is a matrix of coordinates of Bezier control points. The subscript i represents the index of the chosen data points on the body surface, and the subscript n represents the degree of the Bezier curve.

If the number of the chosen data points is M and the degree of the curve is N, $[P(t_i)]$ is M by 2 matrix, $[B_{i,k}(t_i)]$ is an M by $N+1$ matrix and $[V_i]$ is an $N+1$ by 2 matrix for designating x and y coordinates of the two-dimensional curve. Our problem is to find the matrix $[V_i]$ for predetermined $[P(t_i)]$ and $[B_{i,N}(t_i]$. If the number of data points chosen is not equal to $N+1$, i.e. $M \neq N+1$, it is not possible to obtain

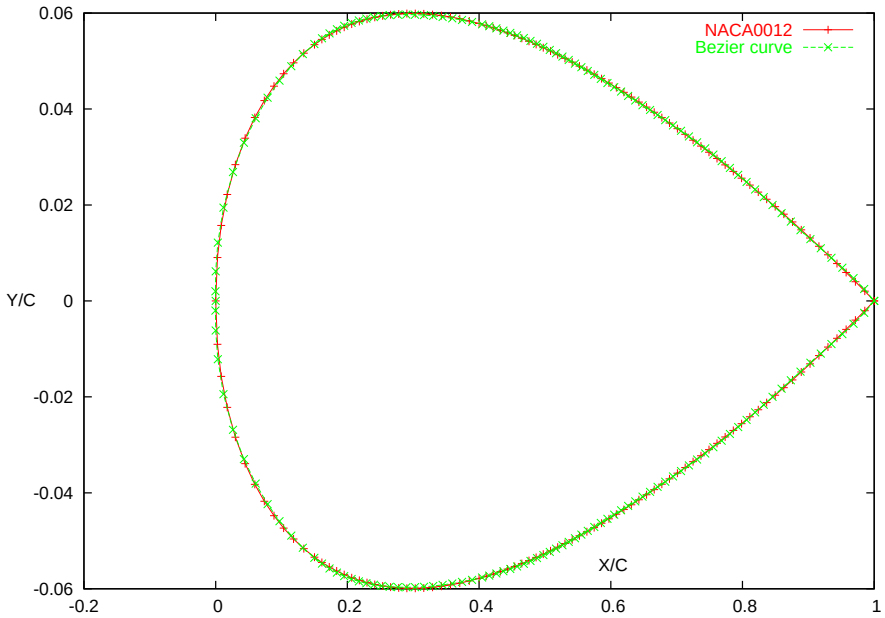

Figure 24: NACA0012 profile and Bezier curve.

the inverse of the matrix $[B_{i,N}(t_i)]$ because this is not a square matrix. To this end we multiply Eq.(3.6) by the transposed of $[B_{i,N}(t_i)]$ and transform it to a square matrix:

$$[V_i] = [[B_{i,N}(t_i)]^T [B_{i,N}(t_)]]^{-1} [B_{i,N}(t_i)]^T [P(t_i)]. \tag{3.7}$$

If the number of data points chosen is equal to $N+1$, i.e. $M = N+1$, it is possible to derive directly the inverse matrix of $[B_{i,N}(t_i)]$ from Eq.(3.6):

$$[V_i] = [B_{i,k}(t_i)]^{-1} [P(t_i)] \tag{3.8}$$

On the basis of the above method for generating a Bezier curve we tested it for the NACA 4-digits airfoils. We take two different Bezier curves for the upper and lower profiles, respectively. The data chosen are as follows:

Profiles: NACA0012, NACA0018, NACA2412, NACA4412

$M = 10$ including leading and end points $P_0(0,0), P_9(1,0)$ for the upper and lower curve, respectively;

$N = 82$ for the upper and lower curves, respectively.

As we can see from these figures, there is no identifiable difference between the original NACA 4-digit profiles and the profiles reconstructed by Bezier curves. Therefore we can apply this method to the Bezier parameterization for the airfoil shape, see Figures 24, 25, 26, and 27.

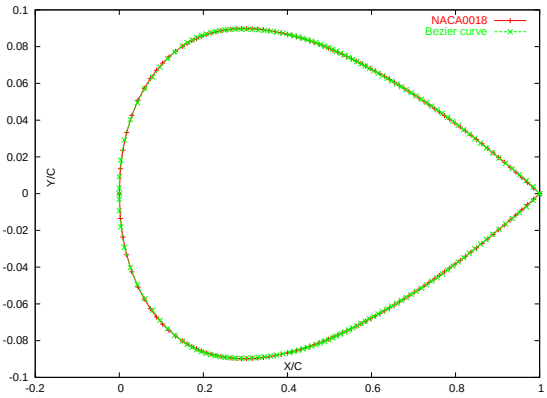

Figure 25: NACA0018 profile and Bezier curve.

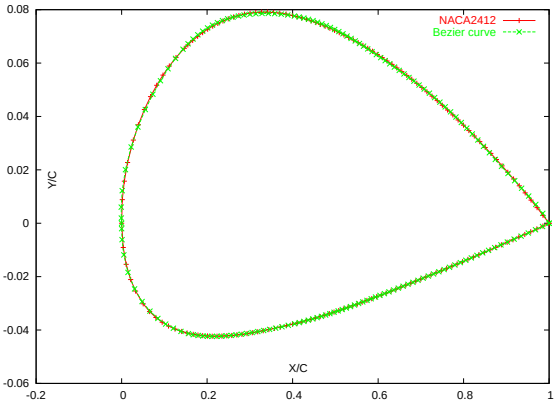

Figure 26: NACA2412 profile and Bezier curve.

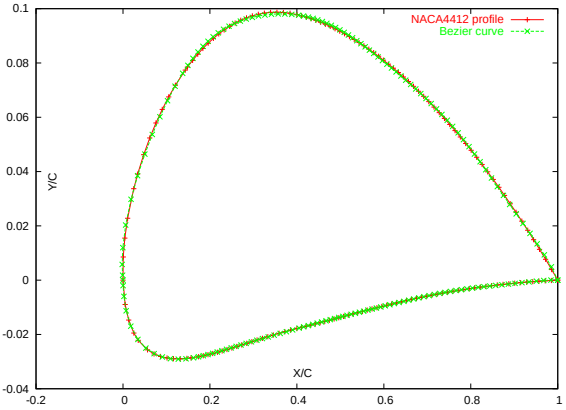

Figure 27: NACA4412 profile and Bezier curve.

3.3 The setting of the shape optimization problem

In this section we formulate the shape optimization for 2-dimensional transonic airfoils by the use of the shape parameterization of Bezier curves and compare the computational results of full potential equation for the NACA 4-digit airfoils and for the profiles reproduced by Bezier curves.

The aerodynamic shape optimization problem consists of determining values of design vareiables, which describe the shape of the airfoil, such that the objective function is minimized subject to constraint equations, which contain the flow equations and other airfoil geometry constraints.

Objective function

For the objective functions we consider the inverse design, lift-constrained drag minimization .

In the inverse design problem the objective function is given by

$$\mathcal{J}_1 = \frac{1}{2} \oint_{\Gamma_P} (C_p - C_p^0)^2 ds, \tag{3.9}$$

where C_p^0 represents the target pressure distribution which is user specified. For the lift-constrained drag minimization we consider the following objective function [42]

$$\mathcal{J}_2 = \mathcal{J}_{2,a} + \mathcal{J}_{2,b}, \tag{3.10}$$

where

$$\mathcal{J}_{2,a} = \omega_D \left(1 - \frac{C_D}{C_D^0}\right)^2 + \omega_L \left(1 - \frac{C_L}{C_L^0}\right)^2, \tag{3.11}$$

$$\mathcal{J}_{2,b} = \begin{cases} \displaystyle\sum_{i=1}^{N_{TC}} \omega_{TC} \left(1 - \frac{t(x_i)}{t^0(x_i)}\right)^2 & \text{if } t(x_i) < t^0(x_i), \\ 0 & \text{otherwise.} \end{cases} \tag{3.12}$$

Here C_D^0 and C_L^0 represent the target drag and lift coefficients, respectively. The weights ω_D and ω_L are specified constants. N_{TC} is the number of thickness constraints, $t^0(x_i)$ is the minimum allowable airfoil thickness at x and ω_{TC} is a user specified constant.

Design variables

Originally, the design variables of the airfoil are the x, y -coordinates of all the points on the profile. The geometry of the airfoil can be parameterized by the control points of the Bezier curve, so that we can choose the control points as the design variables. In our computations we take the y-coordinates of the control points of the Bezier curve as the design variables while the x-coordinates are fixed.

State equation

We take the coupling problem as the state equation:

$$\begin{aligned}
&a(u|u,v) - \langle \lambda, v\rangle = l_1(v,\beta) && \text{for all } v \in V^0,\\
&b(\lambda,\psi) + \langle u,\psi\rangle - d(u,\psi) = l_2(\psi,\beta) && \text{for all } \psi \in H^{-\frac{1}{2}}(\Gamma_\infty),\\
&\int_\Omega \nabla u\cdot\nabla\psi dx \leqslant B\int_\Omega \psi dx && \text{for all } \psi \in C_0^\infty(\Omega) \qquad \text{with } \psi \geqslant 0,\\
&F(\beta) = |\nabla u^+|^2_{TE} - |\nabla u^-|^2_{TE} = 0.
\end{aligned} \tag{3.13}$$

Shape optimization problem

As obtained in Section 2.1, the pressure, lift and drag coefficients are functions of the pressure distribution P, and according to the relationship between velocity potential and pressure, these are also functions of the velocity potential u, .i.e. $C_P(|\nabla u(x)|), C_L(|\nabla u(x)|), C_D(|\nabla u(x)|), \quad x \in \mathbb{R}^2$.

If we denote by $X_D = \{X_D^i\}, i = 1, ..., M$ the design variables, the objective functions $\mathcal{J}_\alpha, \alpha = 1, 2$ can be represented by the following form:

$$\mathcal{J}_\alpha(X_D^i) = \mathcal{J}_\alpha(X_D^i, |\nabla u(X_D^i)|) \quad \alpha = 1, 2, \quad i = 1, ..., M. \tag{3.14}$$

Therefore, we can formulate the shape optimization problem for two-dimensional transonic airfoils as follows:

find $X_{D0} = \{X_{D0}^i\} \in D_{ad}$ satisfying

$$\mathcal{J}_\alpha(X_{D0}) = \min_{X_D \in D_{ad}} \mathcal{J}(X_D) \qquad (OP_0)$$

subject to Eq.(3.13).

Ahead considering the numerical analysis for the shape optimization, we compare the numerical results for the coupling problem on NACA 4-digit airfoils with those belonging to profiles represented by Bezier curves. See Figures 28 and 29.

Character	NACA0012	Bezier curve
Lift coefficient	0.19231292	0.19272575
Drag coefficient	0.00688704	0.00676633394
Circulation	16.1610877	16.180233

Table 3: Comparison of C_L, C_D, L on the NACA0012 and on the Bezier curve for $M_\infty = 0.7$, $\alpha = 1.0$.

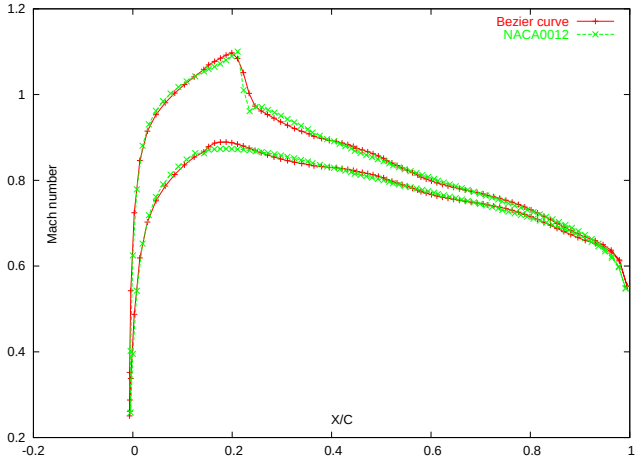

Figure 28: Comparison of Mach number distributions on the NACA0012 profile and on the Bezier curve with $M_\infty = 0.7, \alpha = 1.0$.

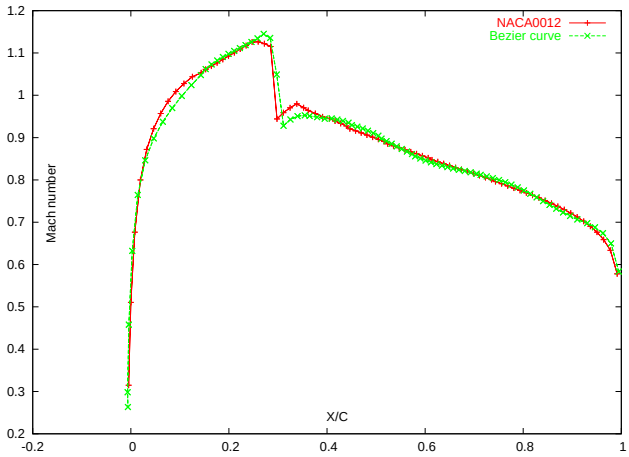

Figure 29: Comparison of Mach number distributions on the NACA0012 profile and on the Bezier curve with $M_\infty = 0.75, \alpha = 0.0$.

Character	NACA0012	Bezier curve
Lift coefficient	$3.26970912E-06$	$4.64935528E-06$
Drag coefficient	0.000279702976	0.000107704941
Circulation	0.000437500021	0.000412500012

Table 4: Comparison of C_L, C_D, L on the NACA0012 and on the Bezier curve for $M_\infty = 0.75$, $\alpha = 0.0$.

3.4 The shape sensitivity analysis for problem (OP_0)

In order to solve the shape optimization problem one needs the shape derivative of the objective function $\mathcal{J}_\alpha$ with respect to the design variable X_D. To this end we use the adjoint state technique here.

Shape derivative evaluation by using the adjoint method

Let us denote by $\mathbb{Q}$ the nodal vector of the discrete solution u_h to the coupling problem (3.13). The discretization of the coupling problem (3.13) can be rewritten in the form of a system of nonlinear algebraic equations:

$$\mathcal{R}(\mathbb{Q}) = C(\mathbb{Q})\mathbb{Q} - \mathbb{F}. \tag{3.15}$$

The gradient of the objective function $\mathcal{J}_\alpha(X_D, \mathbb{Q})$ is given by

$$\frac{d\mathcal{J}_\alpha}{dX_D} = \frac{\partial \mathcal{J}_\alpha}{\partial X_D} + \frac{\partial \mathcal{J}_\alpha}{\partial \mathbb{Q}} \frac{d\mathbb{Q}}{dX_D}. \tag{3.16}$$

In this equation the difficulty is the evaluation of the $\frac{d\mathbb{Q}}{dX_D}$, referred to as the flow sensitivities. In order to compute the flow sensitivities, differentiating eq.(3.15) with respect to the design variables

$$\frac{d\mathcal{R}}{dX_D} = \frac{\partial \mathcal{R}}{\partial X_D} + \frac{\partial \mathcal{R}}{\partial \mathbb{Q}} \frac{\partial \mathbb{Q}}{dX_D} \tag{3.17}$$

and considering that $\frac{d\mathcal{R}}{dX_D} = 0$, we obtain

$$\frac{\partial \mathcal{R}}{\partial \mathbb{Q}} \frac{\partial \mathbb{Q}}{dX_D} = -\frac{d\mathcal{R}}{dX_D}. \tag{3.18}$$

In order to formulate the discrete adjoint method, substitute Eq.(3.18) into Eq.(3.16) to obtain

$$\frac{d\mathcal{J}_\alpha}{dX_D} = \frac{\partial \mathcal{J}_\alpha}{\partial X_D} - \frac{\partial \mathcal{J}_\alpha}{\partial \mathbb{Q}} \left(\frac{\partial \mathcal{R}}{\partial \mathbb{Q}}\right)^{-1} \frac{d\mathcal{R}}{dX_D}. \tag{3.19}$$

Let us define the following intermediate problem:

$$\frac{\partial \mathcal{R}^T}{\partial \mathbb{Q}} \psi = \frac{\partial \mathcal{J}_\alpha^T}{\partial \mathbb{Q}}. \tag{3.20}$$

This is known as the adjoint equation where the vector ψ represents the adjoint variables. Substituting the value of ψ into Eq.(3.19), the gradient becomes

$$\frac{d\mathcal{J}_\alpha}{dX_D} = \frac{\partial \mathcal{J}_\alpha}{\partial X_D} - \psi^T \frac{d\mathcal{R}}{dX_D}. \tag{3.21}$$

The adjoint equation (3.20) is independent of the design variables, while Eq.(3.18) must be solved for each value of the design variables.

The inverse design objective function $\frac{\partial \mathcal{J}}{\partial \mathbb{Q}}$ can be evaluated analytically, while for the drag minimization objective function, the derivative is evaluated using centered

differences. The remaining terms in Eq.(3.21), i.e., the objective function sensitivity $\frac{\partial \mathcal{J}_\alpha}{\partial X_D}$ and the residual sensitivity $\frac{\partial \mathbb{R}}{X_D}$, are also evaluated by the use of centered differences.

The sensitivity analysis for the shape optimization problem (OP_0)

In order to derive the shape sensitivity by using the adjoint state technique, it is necessary to find $\frac{\partial \mathcal{J}_\alpha}{\partial X_D}, \frac{d\mathcal{R}}{dX_D}$, and the solution ψ^T of the adjoint equation (3.20).

We must derive the adjoint equation of the discrete coupling problem

$$\begin{aligned}
&a_h(\tilde{u}_h|\tilde{u}_h,\tilde{v}_h) - \langle\tilde{\lambda}_h,\tilde{v}_h\rangle_h = \tilde{l}_1^h(\tilde{v}_h,\beta_h) && \text{for all } \tilde{v}_h \in \tilde{V}_h,\\
&\tilde{b}_h(\tilde{\lambda}_h,\tilde{\psi}_h) + \langle\tilde{u}_h,\tilde{\psi}_h\rangle_h - \tilde{d}_h(\tilde{u}_h,\tilde{\psi}_h) = \tilde{l}_2^h(\tilde{\psi}_h,\beta_h) && \text{for all } \tilde{\psi}_h \in \tilde{H}_h,\\
&\int_{\Omega_h} \nabla\tilde{u}_h\cdot\nabla\psi_h dx \leqslant B\int_{\Omega_h}\psi_h dx && \text{for all } 0\leqslant\psi_h\in\tilde{V}_h,\\
&F(\beta_h) = |\nabla\tilde{u}_h^+|^2_{TE} - |\nabla\tilde{u}_h^-|^2_{TE} = 0.
\end{aligned} \tag{3.22}$$

Using the definition of the penalty function

$$\mathcal{P}_h(\phi_h) := \frac{\mu}{2}\sum_{\substack{i=1\\ p_i\notin\Sigma\cup\Gamma_\infty}}^{N}\frac{1}{A_i^\epsilon}([-\int_{\Omega_h}\nabla\phi_h\cdot\nabla\omega_{h_i}dx - B\int_{\Omega_h}\omega_{h_i}dx]^+)^2,$$

the discrete coupling problem can be rewritten as follows:

$$\begin{aligned}
&a_h(\tilde{u}_h|\tilde{u}_h,\tilde{v}_h) - \langle\tilde{\lambda}_h,\tilde{v}_h\rangle_h + \mathcal{P}_h'(\tilde{u}_h) = \tilde{l}_1^h(\tilde{v}_h,\beta_h) && \text{for all } \tilde{v}_h \in \tilde{V}_h,\\
&\tilde{b}_h(\tilde{\lambda}_h,\tilde{\psi}_h) + \langle\tilde{u}_h,\tilde{\psi}_h\rangle_h - \tilde{d}_h(\tilde{u}_h,\tilde{\psi}_h) = \tilde{l}_2^h(\tilde{\psi}_h,\beta_h) && \text{for all } \tilde{\psi}_h \in \tilde{H}_h,\\
&F(\beta_h) = |\nabla\tilde{u}_h^+|^2_{TE} - |\nabla\tilde{u}_h^-|^2_{TE} = 0,
\end{aligned} \tag{3.23}$$

where $\mathcal{P}_h'(\tilde{u}_h)$ is the Frechet derivative of the penalty function $\mathcal{P}_h(\tilde{u}_h)$. Thus, we can describe the coupling problem in the same way as Eq.(3.15):

$$\begin{aligned}
\mathcal{R}(\mathbb{Q}) = C(\mathbb{Q})\mathbb{Q} - \mathbb{F} &= \int_{\Omega_h}\varrho(|\nabla\tilde{u}_h|^2)\nabla\xi_h\cdot\nabla\tilde{v}_h dx\\
&+\mu\sum_{\substack{i=1\\ p_i\notin\Sigma\cup\Gamma_\infty}}^{N}\frac{1}{A_i^\epsilon}\left(\int_{\Omega_h}\nabla\tilde{u}_h\cdot\nabla\omega_{h_i}dx - B\int_{\Omega_h}\omega_{h_i}dx\right)^+\left(\int_{\Omega_h}\nabla\tilde{v}_h\cdot\nabla\omega_{h_i}dx\right),
\end{aligned} \tag{3.24}$$

where $\xi_h := \xi_h(\tilde{u}_h,\lambda_h) \in V_h^0$ is defined as the FEM-solution of the variational Poisson equation

$$\int_{\Omega_h}\nabla\xi_h\cdot\nabla\tilde{v}_h dx = a_h(\tilde{u}_h|\tilde{u}_h,\tilde{v}_h) - \langle\lambda_h,\tilde{v}_h\rangle - \tilde{l}_1^h(\tilde{v}_h,\beta_h) \text{ for all } \tilde{v}_h\in\tilde{V}_h^0,$$

and λ_h is the solution of the boundary integral equation

$$\tilde{b}_h(\lambda_h, \tilde{v}_h) = \tilde{l}_2^h(\tilde{v}_h, \beta_h) - \langle \tilde{u}_h, v_h \rangle_h + \tilde{d}_h(\tilde{u}_h, \tilde{v}_h) \text{ for all } \eta_h \in \tilde{H}_h.$$

Note that $\mathcal{P}_h'(\tilde{u}_h)$ is not differentiable with respect to the velocity potential $\tilde{u}_h$ any more. Thus, we use the approximate function $\gamma_\delta(y)$ mentioned in Section 2.
First of all, instead of solving the discrete minimization problem $(\mathcal{P})$ (2.60), we find the solution to its approximate problem $(\mathcal{P}^\delta)$ (2.77) and use $\mathcal{P}_h^\delta(\tilde{u}_h)$ instead of $\mathcal{P}_h(\tilde{u}_h)$. Eventually we can compute the derivatives $\frac{\partial \mathcal{R}}{\partial \mathbb{Q}}$ and $\frac{d\mathcal{R}}{dX_D}$ by using the centered difference formula. Due to the third term of Eq.(3.24), the coefficient matrix of the adjoint equation is asymmetric, and a band matrix whose entries of the side diagonals above and below the main diagonal are $N_{BW} - 1$, respectively, where N_{BW} is the maximal value of differences between vertices of element triangles of the domain Ω_h. Therefore, we use the DGBSL function of the LINPACK Library to solve the adjoint equation.

The points $(X(t_i), Y(t_i)), i = 1, ..., N_p$ on the airfoil surface are described by the Bezier control points $(X_D^j, Y_D^j), j = 1, .., N$,

$$\begin{cases} X(t_i) = \sum_{j=0}^{N} X_D^j B_N^j(t_i), \\ Y(t_i) = \sum_{j=0}^{N} Y_D^j B_N^j(t_i), \end{cases} \tag{3.25}$$

so that we obtain

$$\frac{dX(t_i)}{dX_D^j} = \frac{dY(t_i)}{dY_D^j} = B_N^j(t_i).$$

Thus,

$$\frac{\partial \mathcal{J}_\alpha}{\partial X_D^j} = \frac{\partial \mathcal{J}_\alpha}{\partial X(t_i)} \cdot B_N^j(t_i), \quad i = 1, ..., N_p, \quad j = 1, ..., N,$$

and

$$\frac{d\mathcal{R}}{dX_D^j} = \frac{d\mathcal{R}}{dX(t_i)} \cdot B_N^j(t_i), \quad i = 1, ..., N_p, \quad j = 1, ..., N.$$

Hence, we obtain the shape derivative of the objective function with respect to the design variables according to Eq.(3.21).

3.5 The optmization method and computational algorithm

In this section we present the quasi-Newton method to be used in the shape optimization and the computational algorithm of the shape optimization.

Optimization method

The most popular minimization technique for unconstrained problems is Newton's Method. It is effective, robust and quadratically convergent. In each iteration, the step update is: $x_{k+1} = x_k - (\nabla^2 f_k)^{-1} \nabla f_k$. Therefore, in order to apply Newton's Method it is necessary to evaluate analytically the second derivative and offer to the algorithm. The inverse of Hessian has to be calculated in each iteration, and moreover, in some applications, the calculation of the second derivative is impossible. In our case the second derivative of the objective function with respect to the design variables is not available. The quasi-Newton method enables us to overcome this disadvantage. The quasi-Newton method approximates Hessian or inverse Hessian, and we can solve the optimization without analytical calculation of the second derivative, while the gradients are available.

We consider the following nonlinear unconstrained minimization problem:

$$min f(x), \quad x \in \mathbb{R}^n. \tag{3.26}$$

The general algorithm of quasi-Newton method can be described as follows.

Given x_0 and some initial Hessian approximation B_0 (or an inverse Hessian approximation H_0).

For $k = 0, 1, 2, ...$

Evaluate gradient g_k.
Calculate the update vector s_k by line search or trust region methods.

$$x_{k+1} \leftarrow x_k + s_k$$

$$y_k \leftarrow g_{k+1} - g_k$$

Update B_{k+1} or H_{k+1} according to the quasi-Newton formulae.

End(for).

The basic requirement for the updating formula is that the secant condition is satisfied in each iteration, i.e.,

$$B_{k+1} s_k = y_k. \tag{3.27}$$

We apply the BFGS (Broyden-Fletcher-Goldfarb-Shanno method) [17] as the quai-Newton method to update the Hessian approximation B_{k+1} to our shape optimization problem.

The inverse Hessian update H_{k+1} is obtained by solving the problem:

$$\min_{H} \|H - H_k\|, \quad s.t. \quad H = H^T, Hy_k = s_k. \tag{3.28}$$

The solution of (3.28) gives the inverse Hessian update

$$H_{k+1} = (\mathcal{I} - \varrho_k s_k y_k^T) H_k (\mathcal{I} - \varrho_k y_k s_k^T) + \varrho_k s_k s_k^T \tag{3.29}$$

where

$$\varrho_k = \frac{1}{y_k^T s_k}.$$

The Hessian update can be calculated by using the Sherman-Morrison-Woodbury formula [43] as

$$B_{k+1} = B_k - \frac{B_k s_k s_k^T B_k}{s_k^T B_k s_k} + \frac{y_k y_k^T}{y_k^T s_k}. \tag{3.30}$$

A good initial approximation of the Hessian is often used to improve the performance of the method. The choices usually use preconditioning or scaling as follows:
• The identity matrix I, or some multiple of it, $H_0 = \beta I$

• Some finite difference approximation of the gradient g_k at x_0

• A scaled version of the identity, $H_0 = diag(s_1, s_2, ..., s_n)$, where s_i are scales

• H_0 is rescaled before H_1 is computed as $H_0 = (\frac{y_0^T s_0}{y_0^T y_0})I$ which ensures that H_{k+1} does not get very large.

The BFGS is the most effective quasi-Newton correction. If H_k is positive definite, then so is H_{k+1}, hence if H_0 is chosen to be positive definite, the rest of the H_k will also be positive definite. Also, BFGS has self-correcting properties: if H_k incorrectly approximates the curvature of the objective function and this estimate slows down the iteration, then the inverse Hessian approximation will tend to correct itself during the next few steps. Such advantages of the BFGS motivates us to apply it to our optimization problem.

Computational Algorithm

At last we are prepared to formulate the computational algorithm of the shape optimization for two-dimensional transonic airfoils in the unbounded domain.
The comptational algorithm consists essentially four parts, i.e., the shape parametrization by Bezier curves, the solution of the coupling problem, the shape sensitivity analysis and the shape optimization.

The algorithm reads as follows.
begin

0) Initial geometry and Bezier parametrization

• Choose an initial profile, for example NACA0012 and discretize the given domain Ω.

• Parameterize the upper and lower curves of the given profile by two Bezier curves using the given point data of the profile, and find the Bezier control points (N=16, 8 points for the upper and the lower curves, respectively). Here the leading and trailing edge points are excluded.

1) Redrawing the geometry by Bezier curves

• redraw the profile Γ_p by Bezier control points and discretize the domain Ω.

2) Solution of the coupling prolem

• solve the coupling problem (3.22) by using the approximate discrete minimization method according to the algorithm of Section 1.

3) Shape sensitivity analysis

• compute the value of the objective function.

• compute the partial derivatives of the objective function $\frac{\partial \mathcal{J}_\alpha^T}{\partial \mathbb{Q}}$ with respect to the state variables by the central difference formula.

• compute $\mathcal{R}(\mathbb{Q}) = C(\mathbb{Q})\mathbb{Q} - \mathbb{F}$ by using the solution of the coupling problem.

• generate the adjoint equation

$$\frac{\partial \mathcal{R}^T}{\partial \mathbb{Q}}\psi = \frac{\partial \mathcal{J}_\alpha^T}{\partial \mathbb{Q}}$$

and find its solution ψ.

• compute

$$\frac{\partial \mathcal{J}_\alpha}{\partial X_D}, \frac{d\mathcal{R}}{dX_D}$$

by using the difference formula.

• compute the shape gradient of the objective function with respect to the design variables by

$$\frac{d\mathcal{J}_\alpha}{dX_D} = \frac{\partial \mathcal{J}_\alpha}{\partial X_D} - \psi^T \frac{d\mathcal{R}}{dX_D}.$$

4) Optimization procedure

We denote by SUBROUTINE COMPUTATION( ) the previous procedures 1)-3).

• input the value and shape derivatives of the objective function into the quasi-Newton method BFGS. The subroutine COMPUTATION( ) is used in each line search and the corresponding minimization.

• These procedures will be repeated until the residual of the objective function will reach the given accuracy.

end

3.6 Computational results for the shape optimization

In this section we give some computational results of the shape optimization for a quasi-linear elliptic boundary value problem and for a transonic flow problem.

1) Numerical experiments for a quasi-linear elliptic boundary problem

Before performing the numerical experiment for the transonic flow problem, we applied our numerical algorithm to a elliptic boundary value problem for the accuracy test of our algorithm:

$$\begin{aligned} -div[A(|\nabla u|^2)\nabla u] &= f(x) && \text{in } \Omega \\ u &= 0 && \text{on } \Gamma_\infty \\ \frac{\partial u}{\partial n} &= 0 && \text{on } \Gamma_p, \end{aligned} \tag{3.31}$$

where Ω, Γ_∞, and Γ_p concerning the geometry of the above problem are the same shapes as considered above and $A(|\nabla u|^2)$ also has the same type as the density function in transonic flow. This problem corresponds to the electromagnetic or heat conduction potential problem [35],[44].

The objective function is

$$\mathcal{J}(\Gamma_p) = \oint_{\Gamma_p} |u(x) - u_0(x)|^2 dx, \tag{3.32}$$

where the design variables are the coordinates of points on the boundary Γ_p.

The finite element discretization of problem (3.31) can be written as the following system of nonlinear algebraic equations:

$$C(\mathbb{Q})\mathbb{Q} = \mathbb{F}, \tag{3.33}$$

where $\mathbb{Q}$ is a nodal vector of u_h, $\mu(T)$ is the square of a triangular element T, ϕ_k is a finite element basis function, and

$$C_{ik}(x, \mathbb{Q}) = \sum_{T \in supp(\phi_i) \cap supp(\phi_k)} \mu(T) A_h(|\nabla u_{h|T}|^2) \nabla \phi_i(x) \cdot \phi_k(x) \quad \text{for } i, k = 1, ..., N(h),$$

$$F_k = \int_{\Omega_h} f(x)\phi_k(x) dx.$$

The adjoint equation is represented by

$$(C + B)P = \frac{\partial \mathcal{J}}{\partial \mathbb{Q}}, \tag{3.34}$$

where

$$B_{ik} = \sum_{T \in supp(\phi_i) \cap supp(\phi_k)} \int_T \frac{\partial A}{\partial |\nabla u_{h|T}|^2} (\sum_{m=1}^{3} \nabla u_{h|T} \cdot \nabla \phi_m) \nabla \phi_i \cdot \nabla \phi_k dx.$$

The state equation (3.33) and the adjoint equation (3.34) can be solved by the algorithm described above for the transonic potential problem and our shape optimization algorithm can be applied to this particular problem.

- The first experiment(see Figures. 30, 31, 32).

We choose the NACA0012 profile as initial geometry of Γ_p and the potential values on the NACA0036 profile as the target values. The fig. 1 shows the convergence of the objective function. The value of the objective function lies in the range of 10^{-5} after 20 iterations. Then, the shape of the profile Γ_p and the value of potential on the profile are already similiar to the shape and the value of the target.

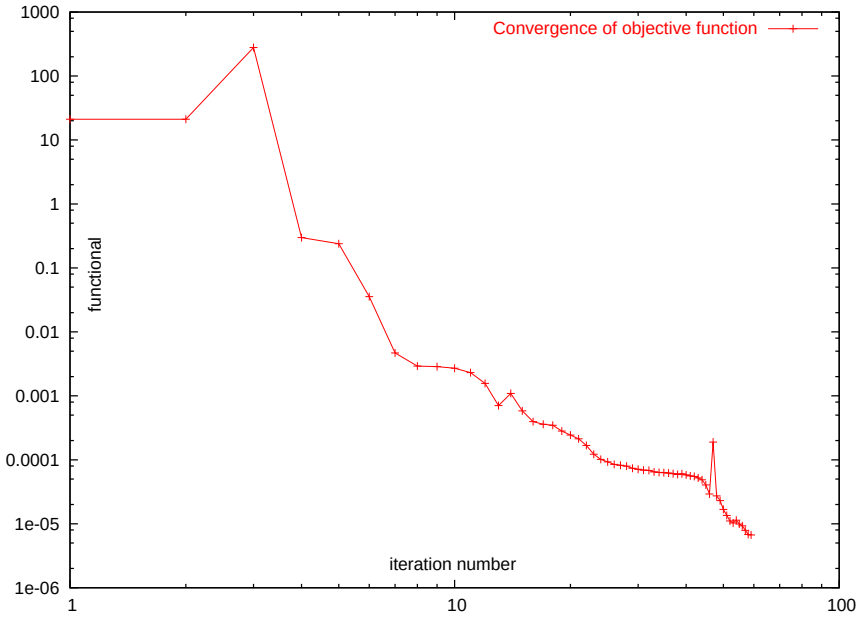

Figure 30: The convergence of the objective function.

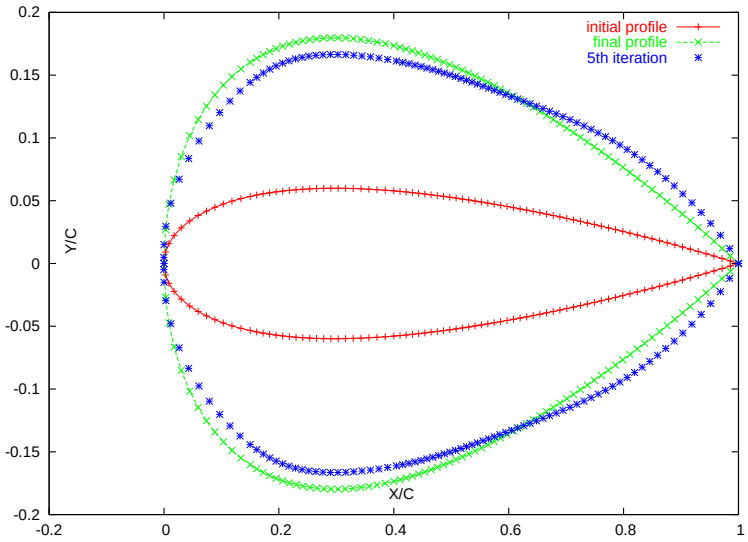

Figure 31: The convergence of the domains.

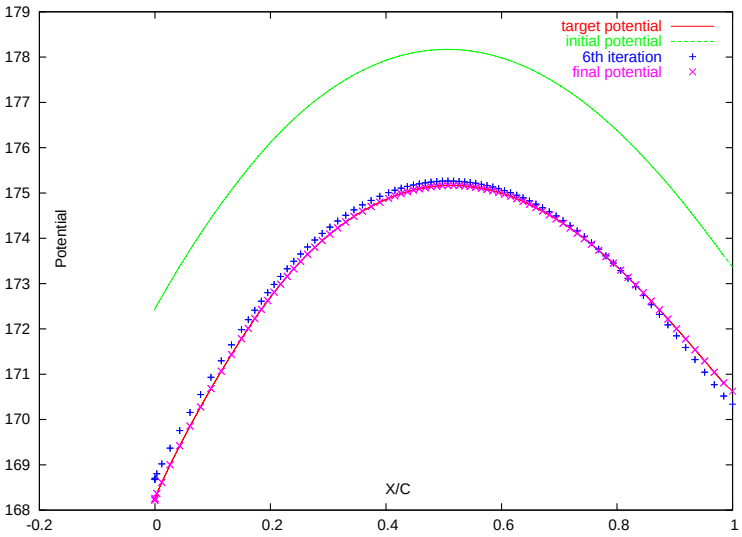

Figure 32: The convergence to the target values.

- The second experiment(see Fig. 33,34,35).

Contrary to the first experiment, in the second experiment we choose the NACA0036 profile as initial geometry and the potential values on the NACA0012 profile as the target values. Although the initial and target data are replaced each other in comparison with the first experiment, the optimization process behaves similiar to the first one.

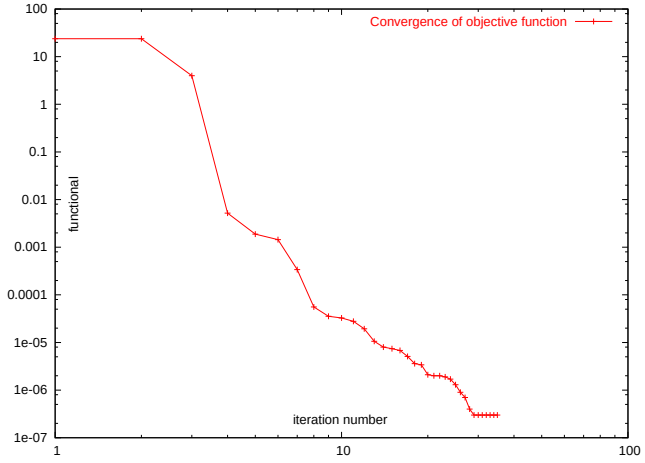

Figure 33: The convergence of the objective function.

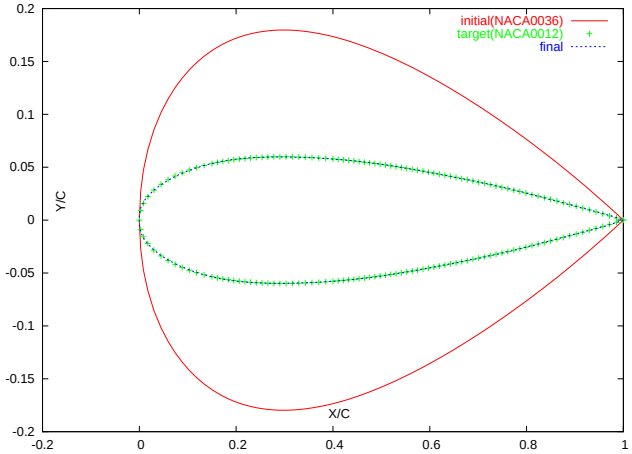

Figure 34: The convergence of the domains.

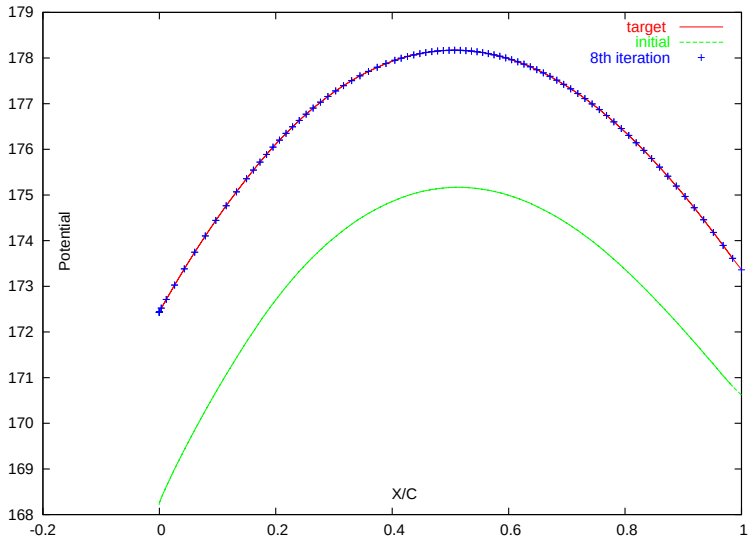

Figure 35: The convergence to the target values.

- The third experiment(see Figures 36, 37 and 38).

In the third experiment we choose the asymmetric profile NACA2412 as initial geometry and the potential values on the NACA0036 profile as the target values. In this case we find that this process performs slightly different from the first and second one. The tendency of the objective function and the values of potential on the profile are the same as for the first and second experiments, but the shape of the profile differs from the target shape. This indicates that the solution of the inverse problem is not unique.

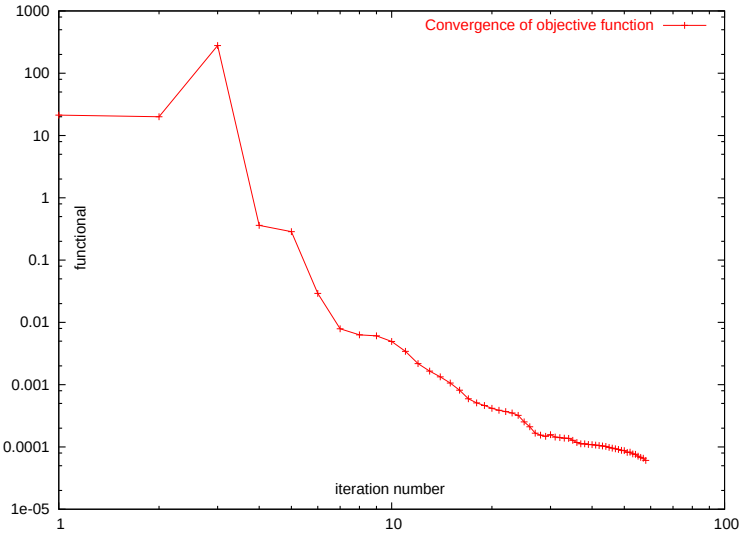

Figure 36: The convergence of the objective function.

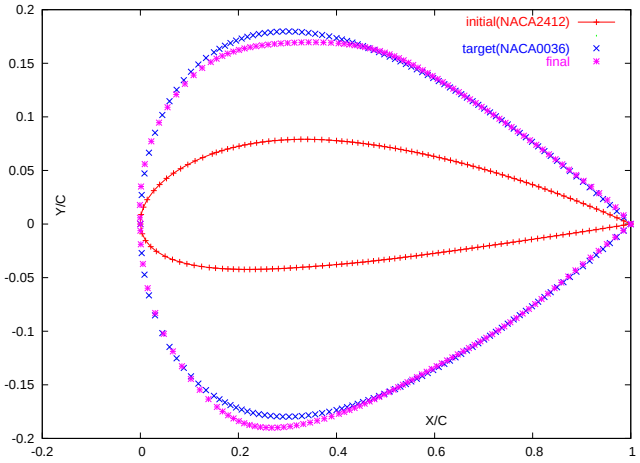

Figure 37: The convergence of the domains.

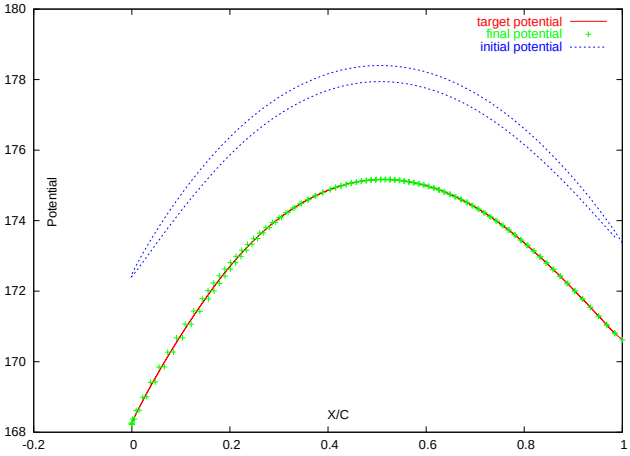

Figure 38: The convergence to the target values.

Throughout these preparatory experiments for the shape optimization of a quasi-linear boundary value problem, we have the confidence that our algorithm can be applied to the shape optimization for the transonic airfoil.

2) Numerical experiment for the transonic flow problem

Here, we present the numerical experiments for the shape optimization of transoinc airfoil with the shape objective functions $\mathcal{J}_\alpha, \alpha = 1, 2$ defined above. The numerical experiments for $\mathcal{J}_1, \mathcal{J}_2$ are performed for the transonic inverse problem and for the lift-constrained drag minimization and lift enhancement problem, respectively.

Numerical experiments for the transonic inverse problem

• NACA0012 airfoil, $M_\infty = 0.55$, $\alpha = 0.0$, target: NACA0018, $\mathcal{J}_1$

Here, The "target: NACA0018" means that we chose the pressure coefficient values on the NACA0018 airfoil as the target values.

The suitable selection of the entropy parameters $\mu, B \geqslant 0$, and the parameter $\delta \geqslant 0$ for the smooth approximation of the penalty function play a crucial role in this experiment. According to our experience, if one chooses $\delta \geqslant 0$ greater than 0.01, the computation will fail. To this end we set $\mu = 5 \cdot 10^{-6}$, $B = 150$, $\delta = 0.001$. The results are shown in the Figures 39, 40 and 41.

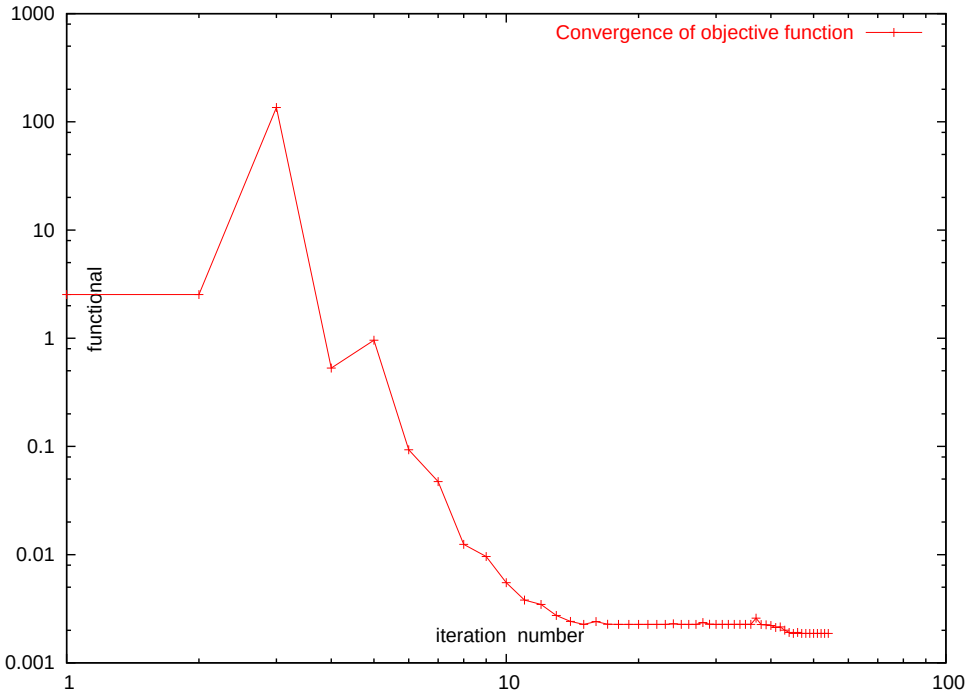

Figure 39: The convergence of the objective function.

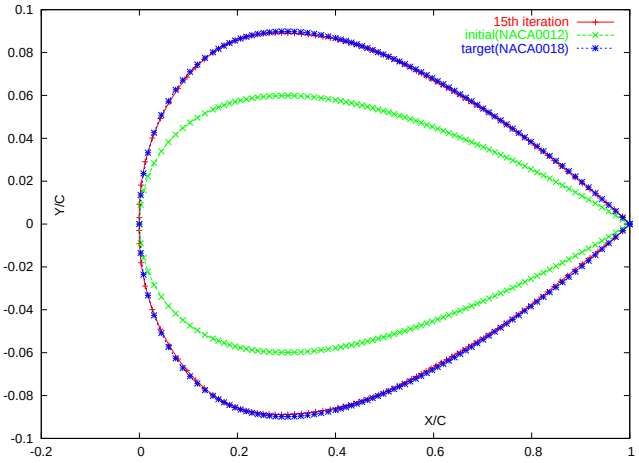

Figure 40: The convergence of the domains.

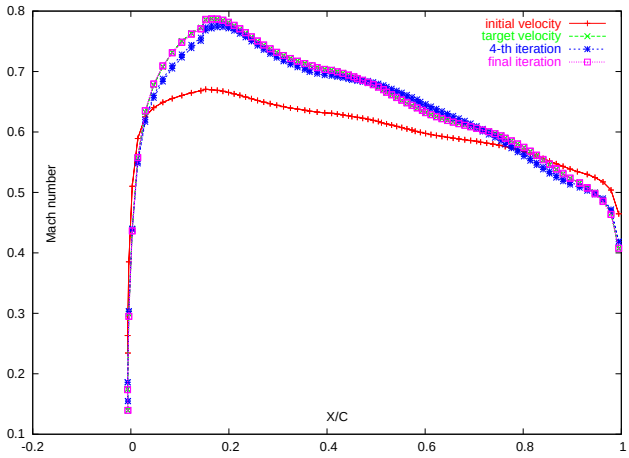

Figure 41: The convergence to the target values.

- NACA0012 airfoil, $M_\infty = 0.55$, $\alpha = 1.0$, target: NACA0015, $\mathcal{J}_1$

In this experiment we set $\mu = 2 \cdot 10^{-6}$, $B = 150$, $\delta = 0.1$, see Figures. 42, 43 and 44.

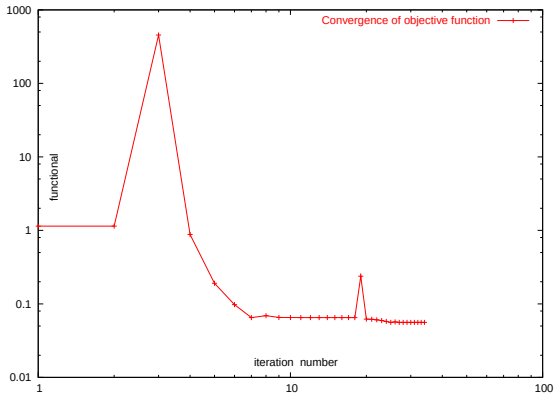

Figure 42: The convergence of objective function.

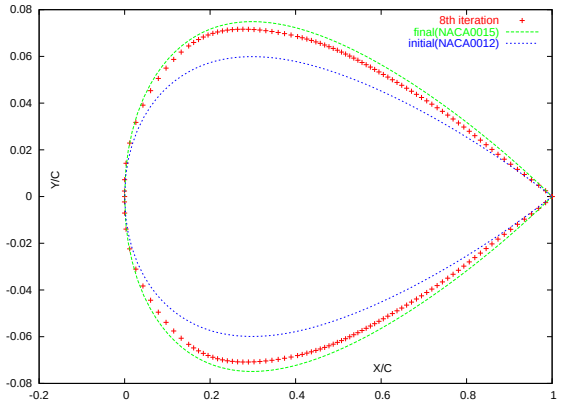

Figure 43: The convergence of the domains.

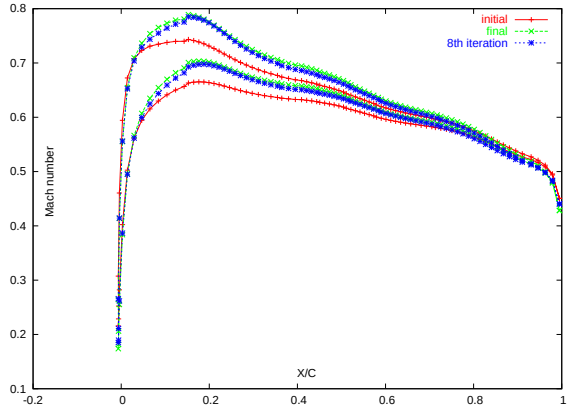

Figure 44: The convergence to the target values.

Numerical experiments for the lift-constrained drag minimization problem

• The first numerical experiment

We take the following functional as the objective function:

$$\mathcal{J}_2 = \omega_L \left(1 - \frac{C_L}{C_L^0}\right)^2 + \omega_D C_D^2. \tag{3.35}$$

Then we choose the NACA 0012 airfoil with $M_\infty = 0.55$, $\alpha = 0.0$, $\delta = 0.0001$ as the initial profile. We set $\omega_L = m_D = 0.5$, $C_L^0 = 0.02$. The below table shows the values of the lift and drag coefficients, circulation and objective function corresponding to the initial and final iterations, respectively.

Iteration	Lift coefficient	Drag coefficient	Circulation	Function
initial	0.00000187	0.00032178	0.00012500	0.4999066
final	0.01999967	0.00032322	1.33925298	0.0000001

Table 5: Evaluation of C_L, C_D, circulation and objective function at initial and final iterations.

Below we show the convergence of the objective function, the shapes of the airfoil at the initial and final iterations and the pressure distributions on the profiles in the figures 45, 46 and 47.

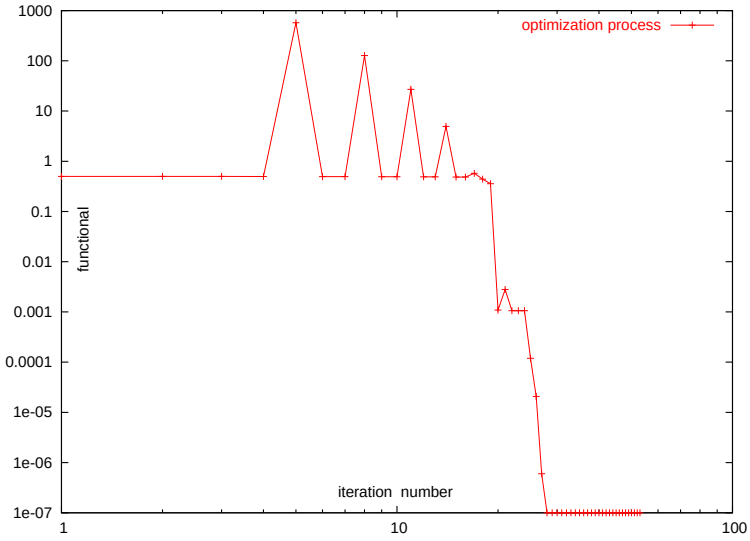

Figure 45: The convergence of the objective function.

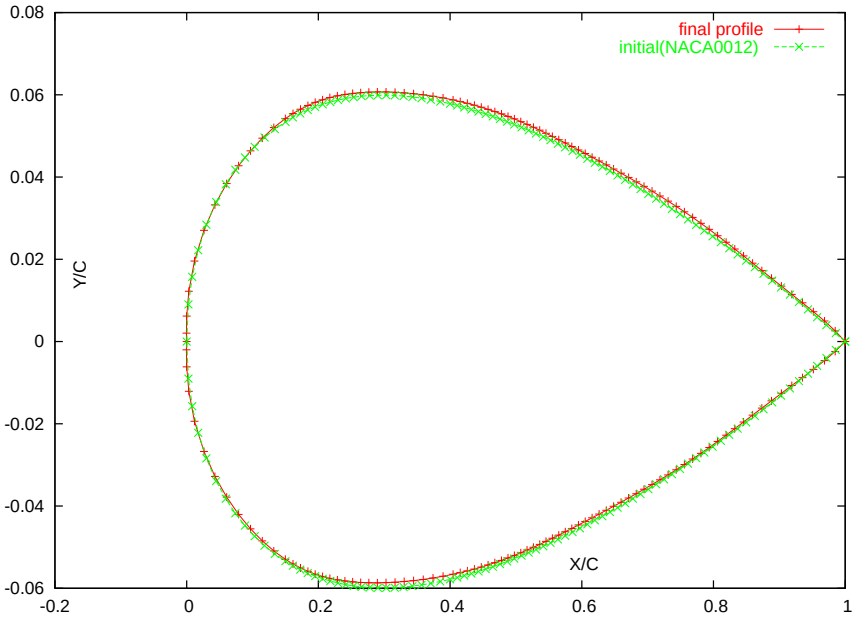

Figure 46: The shapes of airfoil at initial and final iterations.

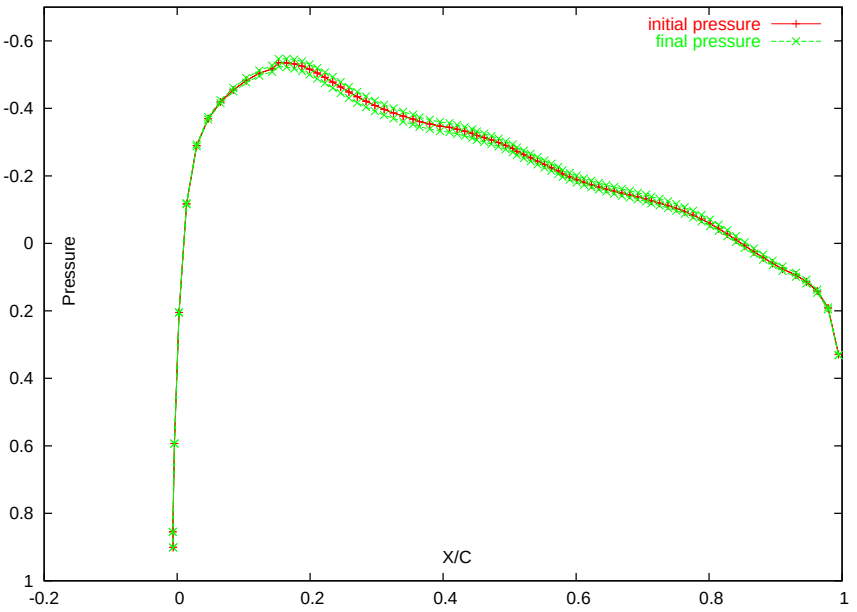

Figure 47: The pressure distributions at initial and final iterations.

• The second numerical experiment

we choose the NACA 0012 airfoil with $M_\infty = 0.75$, $\alpha = 0.0$, $\delta = 0.001$ as the initial profile. We set $\omega_L = m_D = 0.5$, $C_L^0 = 0.5$. As shown in the table below, the initial airfoil is a symmetric profile, so that the lift coefficient and circulation is close to 0. After the optmizaiton process, the lift coefficient is close to the target value 0.5 and the drag coefficient is decreased.

Iteration	Lift coefficient	Drag coefficient	Circulation	Function
1	0.00000486	0.00001422	0.00043750	0.24999903
2	0.00000771	0.00001671	0.00068746	0.24999846
3	0.03619011	0.00014973	1.22177631	0.22302392
4	0.06498839	0.00013138	8.33519736	0.19472556
5	0.13568299	0.00015672	15.1765369	0.06431180
6	0.36175970	0.00016035	29.2204682	0.02430265
7	0.43618244	0.00017512	36.2210535	0.00173025
8	0.47618126	0.00018617	40.2210733	0.00023025
9	0.49117792	0.00019518	43.2207090	0.00003430
10	0.49361801	0.00019420	45.2208677	0.00002343
11	0.50289085	0.00019155	45.2204774	0.00002302

Table 6: Evaluation of C_L, C_D, circulation and objective function at each iteration.

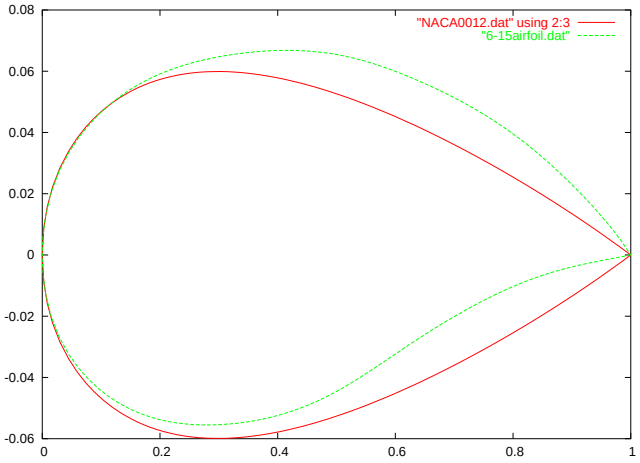

Figure 48: The shapes of airfoil at initial and final iterations.

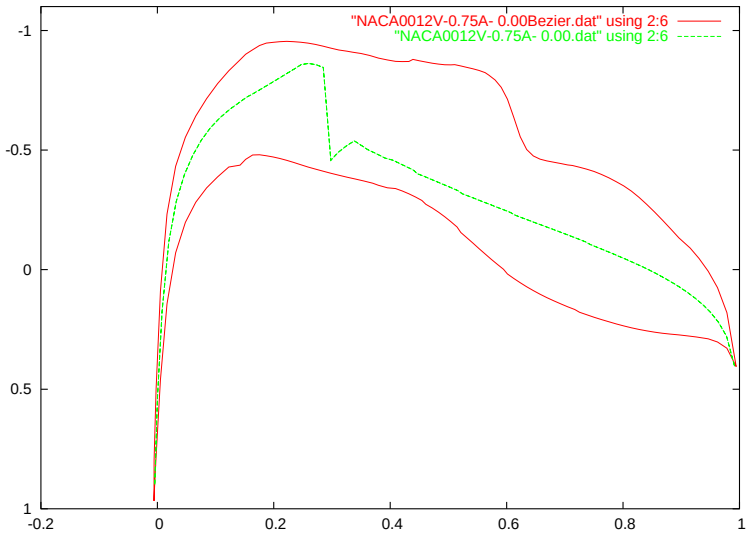

Figure 49: The pressure distributions of initial and final iterations.

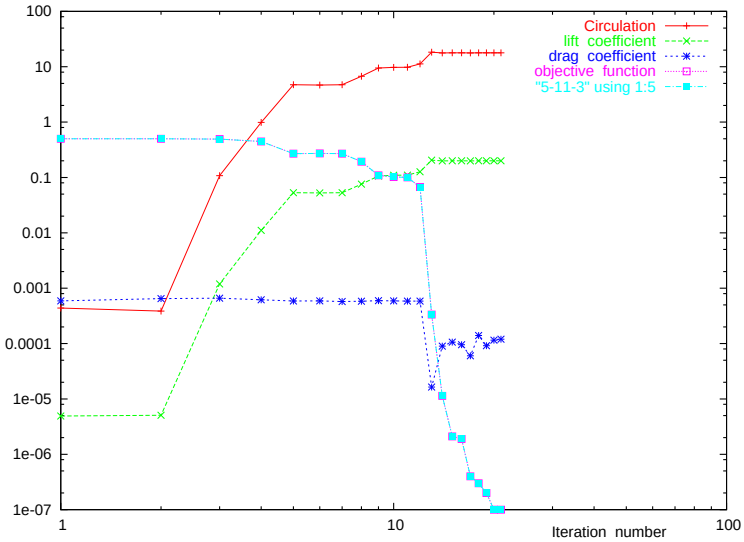

Figure 50: C_L, C_D, circulation and objective function at each iteration.

4 Concluding remarks

In this thesis we proposed a computational algorithm for the shape optimization of the trnsonic airfoil by using the coupling of FEM and BEM based on enough a lot of computational experiments for the transonic fluid flow around the airfoil.
In the numerical experiments for the shape optimization the suitable choices of the entropy constants μ and B, approximation constant δ depending on the shape of the airfoil and travelling velocity are crucial. These choices is obtained from enough numerical experiments. The algorithm and program considered above can be applied to the shape optimization of some nonlinear elliptic boundary value problem with slight modifications. Here we dealt with the aerodynamical design problem for the simplest model of transonic fluid flow. For more applications one should consider the aerodynamical design problem whose state problem is the Euler equation. And for the computational accuracy and speed one should introduce the adaptive mesh generation.

Zusammenfassung

In dieser Arbeit wurde die Form Optimierung fr zwei dimensionale transsonische Flgel mit einer Koppelung von FEM und BEM betrachtet. Die Form Optimierung basiert auf einer exakten numerischen Lsung der Zusatandsgleichung, die das Modell beschreibt. Daher wurden zuerst die Zustandsgleichung und ihre Variationsformulierung hergeleitet und anschlieend die Lsung durch eine Kopplung von FEM und BEM berechnet.

Das mathematische Modell, das hier betrachetet wird ist eine gekoppeltes Randwertproblem mit der vollen Potentialgleichung im inneren Gebiet, der linearisierten Prandtl-Glauert Gleichung im ueren Gebiet, Kopplugsbedingungen auf dem Kopplungsgebiet und der Entropieungleichung. Die diskrete Variaonsformulierung fr das gekoppelte Randwertproblem unter Verwendung von FEM und BEM kann reduziert werden auf ein diskretes Minimierungsproblem. Im Falle transsonischer Strmungen korrespondiert die Straffunktion mit der Entropieungleichung und wird zum Minimierungsfunktional addiert. Das Minimierungsproblem wurde mit der konjugierten Gradientenmethode gelst. Die Entropie-und die Strafparameter, die im Mimimierungsfunktional enthalten sind hngen von der Form des Flgels und der Geschwindigkeit ab. Bei den numerischen Beispielen wurden hierfr verschiedene Parameter gewhlt, die fr verschiedene Formen der Flgel , Geschwindigkeiten und Angriffswinkel stehen.

Danach musste, um die Form Optimierung lsen zu knnen, die adjungierte Zusandsgleichung hergleitet werden. Dazu war es ntig, die zweiten Ableitungen nach dem Geschwindigkeitspotential des Minimierungs Funktionals zu berechnen. Mit Hilfe der adjungierten Zustandsgleichungen konnte der Form Gradient bestimmt werden. Danach wurde die Approximationsfunktion, die von einigen angenherten Parametern abhngt definiert und ausgehend von dieser Funktion das Nherungsproblem des ursprnglichen Minimierungsproblems berechnet. Es wurde gezeigt, dass die Folge von Lsungen der Nherung des diskreten Minimierungsroblems, unter gewissen Bedingungen, gegen die Lsung des stetigen gekoppelten Randwertproblems konvergiert. Gewhnlich wird die Parametrisierung des Flgels mit Bezier Kurven oder B-spline Kurven im rodynamischen Design durchgefhrt, um die Zahl der Konstruktionsvariablen zu reduzieren und man erhlt eine physikalisch realistische Form des Flgels. Im Rahmen der Arbeit wurde ein Algorithmus zur Darstelllung des Flgels mit Hilfe von Bezier Kurven hergeleitet und es wurden numerische Ergebnisse darauf gezeigt. Es wurde die Formsensibilitt Analysis Formel mit Hilfe der diskreten Adjungierten Zustandstechnik gefunden. Basierend auf den obigen Vorbereitungen konnte ein rechenbarer Algoithmus fr die Form Optimierung des zweidimensionalen transsonischen Flgels mit Hilfe der Kopplung von FEM und BEM aufgebaut werden und einige numerische Ergebnisse fr das Inverse Modellierungsproblem und eine vom Auftrieb abhngige Widerstandsminimierung wurden gezeigt. Der Algorithmus, der im Rahmen der Arbeit fr die Form Optimierung betrachtet wurde, kann auf viele Potentialprobleme, inklusive nichtlinearer elliptischer Randwertprobleme angewandt werden.

References

[1] F. Angrand: Optimum design for potential flows, Int. J. Num. Mech. Fluids, **3** (1983), 265-282.

[2] H. Berger: A convergent finite element formulation for transonic flows, Nummer. Math. **56** (1989), 425-447.

[3] H. Berger: Finite-Element-Approximationen für transsonische Strömungen, Doctoral Thesis, Universität Stuttgart, Germany,1989.

[4] H. Berger and M. Feistauer: Analysis of the finite element variational crimes in the numerical approximation of transonic flow. Math. Comp. **61** (1993), 493-521.

[5] H. Berger, G. Warnecke and W. L. Wendland: Analysis of a FEM/BEM coupling method for transonic fow computations, Math. Comp. **66** (1997), 1407-1440.

[6] H. Berger, G. Warnecke and W. L. Wendland: Finite elements for transonic potential flows, Numer. Meth. Part. Diff. Eqns. **6** (1990), 17-42.

[7] V. Braibnt and C. Fleury: Shape optimal design using B-spline, Comput. Meth. Appl. Mech. Engrg. 44 (1984), 247-267.

[8] G. W. Burgreen and O. Baysal: Three Dimensional Aerodynamic Shape Optimization Using Discrete Sensitivity Analysis, AIAA Journal, **34** (1996) 9, 1761-1770.

[9] C. Carstensen and E. P. Stephan: Adaptive coupling of boundary elements and finite elements, RAIRO Anal. Num. **29** (1995) 7, 779-817.

[10] D. Chenals: On the existence of a solution in a domain identification problem, J. Math. Anal. Appl. **52** (1975), 189-289.

[11] P. G. Ciarlet: The Finite Element Method for Elliptic Problems, North-Holland, Amsterdam, 1978.

[12] C. A. Coclici: Domain decomposition methods and far-field boundary conditions for two-dimensional compressible flows around airfoils, Doctoral Thesis, Mathematical Institute A, University of Stuttgart (1998).

[13] C. A. Coclici and W. L. Wendland: On the Treatment of the Kutta-Joukowski Condition in Transonic Flow Computations, ZAMM **79** (1999) 8, 507-534.

[14] C. A. Coclici and W. L. Wendland: Analysis of a heterogeneous domain decomposition for compressible viscous flow, Math. Methods Appl. Sci. **11** (2001), 565-599.

[15] M. Djaoua: A method of calculation of lifting flows around two-dimensional corner-shaped bodies, Math. Comp., **36** (1981), 405-425.

[16] M. Feistauer and J. Nečas: On the Solvability of Transonic Potential Problems, Z. Anal. Anw. **4** (1985) 4, 305-329.

[17] R. Fletcher: Practical Methods of Optimization,Chichester : Wiley; 1987.

[18] G. N. Gatica and G. C. Hsiao: The coupling of boundary element and finite element methods for a nonlinear exterior boundary value problem, Numer. Math. **61** (1992), 171-214.

[19] G. N. Gatica and G. C. Hsiao: The coupling of boundary element and finite element methods for a nonlinear exterior boundary value problem, Z. Anal. Anw. **8** (1989), 377-387.

[20] L. Gebhardt, D. Fokin, T. Lutz and S. Wagner: An implicit-explicit Dirichlet-based field panel method for transonic aircraft design, AIAA paper **2002-3145** (2002), 1-13.

[21] H.-P. Gittel: Studies on Transonic Flow Problems by Nonlinear Variational Inequalities, Z. Anal. Anw. **6** (1987) 5, 447-458.

[22] R. Glowinski and O. Pironneau: On the computation of transonic flows, In: FUJITA, H. (ed.): Funct. Anal. and Num. Anal. Jap. Soc. Prom. Sci., Tokyo-Kyoto 1978, 143-173.

[23] U. Göhner: Adaptive Finite-Element-Methoden für transsonische Strömungen, PhD Thesis, Universität Stuttgart.

[24] U. Göhner and G. Warnecke: A shock indicator for adaptive transonic flow computations, Numer. Math. **66** (1994), 423-448.

[25] U. Göhner and G. Warnecke: A second order finite difference error indicator for adaptive transonic flow computations, Numer. Math. **70** (1995), 129-161.

[26] H. Han: A new class of variational formulations for the coupling of finite and boundary element methods, J. Comput. Math. **8** (1990), 223-232.

[27] J. Haslinger and J. Loišek: Domain Optimization Problem Governed by a State Inequality with a "Flux" Cost Functional, ZAMM **66** (1986), 12, 607-614.

[28] J. Haslinger and P. Neittaanmäki: On Optimal Shape Design of Systems Governed by Mixed Dirichlet-Signorini Boundary Value Problems, Math. Meth. Appl. Sci. **8** (1986), 157-181.

[29] J. Haslinger and P. Neittaanmäki: Penalty method in design optimization of systems governed by a unilateral boundary value problem, Ann. Fac. Sci. Tolouse **V** (1983), 199-216.

[30] J. Haslinger and P. Neittaanmäki: On the existence of optimal shape in contact problems, Numer. Func. Ana. and Optimiz. **7** (1984-1985) 3, 107-124.

[31] J. Haslinger, P. Neittaanmäki, and Salmejoki K: Sensitivity Analysis for some Optimal Shape Design Problems, Z. angew. Math. Mech. 67 (1987) 5, T403-T405.

[32] I. Hlavaček and I. Nečas: Optimization of the domain in ellptic boundary value problems by finite element method, R.A.I.R.O., Numer. Anal. **16** (1982), 351-373.

[33] G. C. Hsiao, Newark, Delaware, P. Kopp and W. L. Wendland: Some Applications of a Galerkin-Collocation method for Boundary Integral Equations of the First Kind, Math. Meth. in the Appl. Sci. **6** (1984), 280-325.

[34] B. L. Keyfitz and G. Warnecke: The existence of viscous profiles and admissibility for transonic shocks, Commun. PArt. Diff. Eqns., **16** (1991), 1197-1221.

[35] M. Kuhn, O. Steinbach: Symmetric coupling of finite and boundary elements for exterior magnetic field problems. Math. Methods Appl. Sci. **25** (2002), 357-371.

[36] R. A. E. Mäkinen: Optimal Shape Design for Transonic Potential Flows, In:K. Morgan, E. Oate, J. Periaux, J. Peraire and O. C. Zienkiewicz (eds.): Finite Elements in Fluids, CIMNE / Pineridge Press 1993.

[37] R. A. E. Mäkinen: Finite element design sensitivity analysis for non-linear potential problems, Commun. Appl. Numer. methods, **6** (1990), 343-350.

[38] J. Mandel and J. Nečas: Convergence of finite elements for transonic potential flows, SIAM J. Numer. Anal **24** (1987) 5, 985-996.

[39] F. Mignot and J. P. Puel, Optimal control in some variational inequalities, SIAM J. Cont. and Optmz. **22** (1984) 3, 466-476.

[40] P. Mund and E. P. Stephan: An adptive two-level method for the coupling of nonlinear FEM-BEM equations, SIAM J. Numer. Analysis, **36** (1999), 1001-1021.

[41] P. Neittaanmäki, J. Sokolowski and J.-P. Zolesio: Optimization of the Domain in Elliptic Variational Inequalities, Appl. MAth. Optim. **18** (1988), 85-98.

[42] M. Nemec and D. W. Zingg: Towards efficient aerodynamic shape optimization based on the Navier-Stokes equations, AIAA-2001-2532, AIAA Computational Fluid Dynamics Conference, 15th, Anaheim, CA, June 11-14, 2001.

[43] Jorge Nocedal and Stephen J. Wright: Numerical optimization, New York: Springer, 1999.

[44] K. Salmenjoki, Neittaanmäki and G. Arumugam: Optimal Shape Design of an Electromagnet, Z. angew. Math. Mech. **69** (1989) 4, T234-T237.

[45] Myong H. Sohn and Kyu J. Lee: Bezier Curve Application in the Shape Optimization of Transonic Airfoils, AIAA paper, **2000-4523** (2000), 883-893.

[46] J. Sokolowski: Introduction to shape optimization, Springer, 1992.

[47] J. Sokolowski: Sensitivity Analysis of Contact Problems with Prescibed Friction, App. Math. Optim. **18** (1988), 99-117.

[48] J. Sokolowski and J.-P. Zolesio: Shape sensitivity analysis of unilateral problems, SIAM J. Math. Anal. **18** (1987) 5, 1416-1437.

[49] A. Sommerer, T. Lutz and S. Wagner: Design of Adaptive Transonic Airfoils by Means of Numerical Optimisation, In: Proceedings of COMAS 2000, European Congress on Computational Methods in Applied Science and Engineering, 11-14 September, (2000), Barcelona, Spain, 2000.

[50] A. Sommerer, T. Lutz and S. Wagner: Numerical Optimisation of Adaptive Transonic airfoils with Variable Camber, In:Proceedings of the 22nd International Congress of the Aeronautical Sciences, 27 August -1 September, (2000), Harrogate, UK, 2000.

[51] O Steinbach: On the stability of the L_2 projection in fractional Sobolev spaces, Numer. Math. **88** (2001) 367-379.

[52] O Steinbach: On a generalized L_2 projection and some related stability estimates in Sobolev spaces, Numer. Math. **90** (2002), 775-786

[53] Z. L. Tang and J.-A. Désidéri: Towards Self-Adaptive Parameterization of Bézier Curves for Airfoil Aerodynamic Design, Rapport de Recherche **4572**, INRIA, September 2002.

Lebenslauf

Allgemeine Angaben

Name	Chol Gyu O
Geburtsdatum	08. Januar 1976
Geburtsort	Pjoengjang, Demokratische Volksrepublik Korea
Staatsangehrigkeit	Koreaner
Familienstand	verheiratet

Werdegang

1983 - 1987	Grundschule in Pjoengjang, DVR Korea
1987 - 1992	Gymnasium in Pjoengjang
1992 - 1998	Universität der Wissenschaft in Pjoengjang
1998 - 2001	Aufbaustudium, Institut für Mathematik, Akademie der Wissenschaft DVR Korea
August 2001	Abschlußprüfung. Diplomarbeit (Msc)
2001-2004	Wissenschaftler, Institut für Mathematik, Akademie der Wissenschaft DVR Korea
Mai 2004 - Juni 2006	Stipendiat Gottlieb Daimler und Karl Benz Stiftung (Mathemtischen Institut A, Universität Stuttgart)